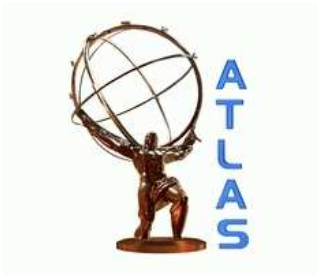

ATLAS NOTE

ATL-PHYS-PUB-2007-XXX

May 30, 2008

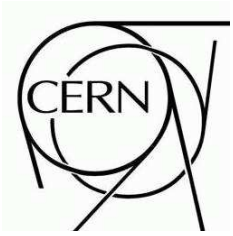

Prospect for single top cross-section measurements in ATLAS

B. Clément[1], J. Cochran[2], C. Cojocaru[3], M. Cristinziani[4], J. Donini[1], J. L. Holzbauer[5], M. Khakzad[3], G. Khoriauli[4], A. Lucotte[1], B.G. Pope[5], P. Ryan[5], A. Shibata[6], D. Schouten[7], R. Schwienhorst[5], N. Triplett[2], K. Yamanaka[2]

[1] CNRS/IN2P3 & UJF/ENSPG, LPSC, Grenoble, France
[2] Iowa State University, Ames IA 50011-3160
[3] Carleton University, Canada
[4] Physikalisches Institut, Bonn University, Germany
[5] Michigan State University, USA
[6] New York University, USA
[7] Simon Fraser University, Burnaby, BC, Canada

Abstract

At the LHC, the production of single top quarks accounts for a third of the top pairs production. With more than two millions of single top events produced every year during a low luminosity run, a precise determination of all contributions to the total single-top cross-section seems achievable. These measurements will lead to the first direct measurement of V_{tb} at the few percent level of precision, and constitute a powerful probe for new physics, via the search for evidence of anomalous couplings to the top quark or the measurements of additional bosonic contributions to the single top production.

The single top production mechanism proceeds through three different sub-processes resulting in distinct final states, topologies, and backgrounds. Given the level of backgrounds affecting the individual selections and the importance of the systematic uncertainties, the use of sophisticated methods appears mandatory to reach evidence and to determine precisely the cross section. This report presents the methods developed to optimize the selection of single top events in the three channels and establishes the ATLAS potential for the cross section measurements for the early data period and for a 30 fb^{-1} low luminosity run.

Contents

1 Introduction **3**

2 Phenomenology of single top analyses **3**
2.1 Single top production 4
2.2 Top pair production 5
2.3 W+jets production 6
2.4 Di-boson production 7
2.5 QCD background 7

3 Simulation techniques, triggers and performance **7**
3.1 Detector simulation 7
3.2 Leptons, jet and missing energy reconstruction 8
3.3 Performance of b-tagging in full and fast simulation 10
3.4 Trigger for single top events 11

4 Strategies for estimating systematic uncertainties **14**
4.1 Introduction 14
4.2 Propagation and combination of errors 14
4.3 Experimental systematic uncertainty 15
4.4 Theoretical and MonteCarlo systematic uncertainties 16

5 Single top event preselection **20**
5.1 Triggering and event preselection 20
5.2 Preselection effi ciency 21
5.3 Strategy to remove QCD background 21

6 Measurement of the t-channel cross section **25**
6.1 Cut based event selection 25
6.2 Systematic uncertainties 27
6.3 Multivariate event selection 30
6.4 Sensitivity at 1 fb^{-1} and the measurement of $|V_{tb}|$ 32
6.5 Summary 33

7 Measurement of the s-channel cross section **34**
7.1 Sequential cut analysis 34
7.2 Likelihood selection 35
7.3 Systematic uncertainties 39
7.4 Summary 40

8 Measurement of the Wt-channel cross section **42**
8.1 Sequential cuts analysis 42
8.2 Boosted decision tree analysis 43
8.3 Systematic uncertainties 47
8.4 Summary 49

9 Single top evidence with the early data **50**
9.1 Event selection 50
9.2 Significance and luminosity 50
9.3 Systematics estimation 51
9.4 Additional variable selection 52
9.5 Results 54

10 Conclusion **55**

1 Introduction

The top quark is one of the key particles in the quest for the origin of particle mass. In particular the electroweak interaction of the top quark is sensitive to many types of new physics. Electroweak production of top quark leads to a final state of a single top quark plus other particles. The production cross section is sensitive to contributions from new particles such as new heavy bosons W' or charged Higgs bosons H^+, and other processes such as flavor-changing neutral currents also result in a single top quark final state [1]. Furthermore, single top production is an important background to many searches for new physics.

The D0 [2] and CDF [3] collaborations at the Fermilab Tevatron reported evidence for single top quark production and a first direct measurement of the CKM matrix element $|V_{tb}|$. This involved advanced analysis methods to extract the small single top quark signal out of the large backgrounds. The Tevatron experiments will collect several fb^{-1} of data, and expect to not only observe single top quark production at the 5 sigma level but also separate two different production modes (s-channel and t-channel). However, the single top production cross section is small at Tevatron energies and single top measurements will be limited by statistics.

At the LHC, the number of signal events is not a problem anymore. The LHC will not only be a strong interaction top quark factory but will also produce several million single top quark events. The cross section for all three modes of single top quark production as well as the CKM matrix element $|V_{tb}|$ can be measured with high precision. Once the single top quark signal has been established, detailed measurements of the process will follow, for example of top quark polarisation, ratios of cross sections, and charge asymmetries. Searches in each of the single top quark channels are sensitive to new physics even before the SM single top signal is found. The D0 collaboration has published limits on W' boson production and flavour changing neutral currents [4, 5].

This paper describes the cross section measurements for the three single top quark production modes and is organised as follows: The single top quark phenomenology is introduced in Section 2, followed by ATLAS object reconstruction and trigger selection respectively in Section 3. All studies are based on a common event preselection, presented in Section 5. As the analyses are designed to minimize the systematics uncertainties affecting the selections, the strategies defined to assess them are described in Section 4. The cross section measurements for the t-channel, s-channel, and Wt-channel are then presented in Sections 6, 7, and 8. Section 9 examines the potential for single top quark studies with early data, and conclusions are given in Section 10.

2 Phenomenology of single top analyses

This section summarises the single top phenomenology and Monte Carlo (MC) event generators used to produce the samples analysed in this paper. While some processes are only generated at the leading order (LO) accuracy, many of them have implemented improvements by methods such as resummation of next-to-leading log terms and some are even calculated at the full next-to-leading order (NLO) accuracy. All

cross-sections are normalised using “K-factors”, to the NLO theoretical calculations whenever available. Most events were generated using a matrix-element (ME) generator and they interfaced to Pythia [6] or Herwig [7] in order to provide additional physics effects such as parton-shower (PS)[1], hadronization and multiple-interactions.

2.1 Single top production

In the standard model single-top production is due to three different mechanisms: (a) W-boson and gluon fusion mode, which includes the t-channel contribution and is referred to as t-channel as a whole (b) associated production of a top quark and a W-boson, indicated as Wt-channel and (c) s-channel production coming from the exchange of a charged boson W^*. The corresponding diagrams are shown in Fig. 1. We note however that these definitions are valid only at a leading order level of corrections: next to leading order (NLO) calculations may indeed lead to the presence of graphs common to those three mechanisms. The total NLO cross-section for all three mechanisms amounts to about 320 pb at the LHC. Among those channels, the dominant contribution comes from the t-channel processes, which account for about 246.6±10.2 pb [8] [9]; the Wt-channel contribution amounts to about 66.5±3.0 pb [10] while the s-channel is predicted with a cross-section of about 10.65±0.65 pb [8] [9].

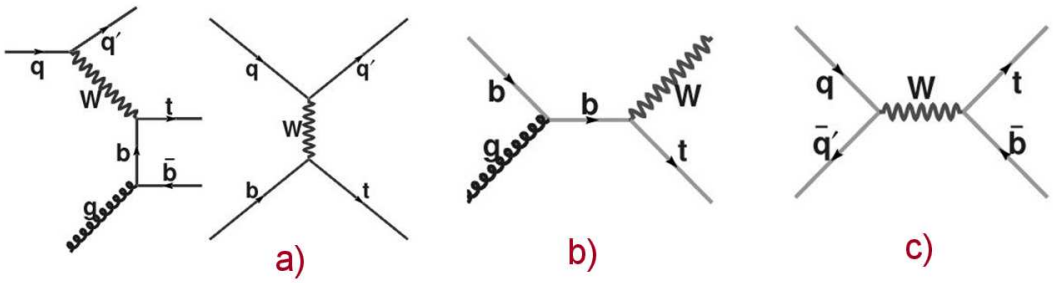

Figure 1: Main graphs corresponding to the three production mechanisms of single-top events: (a) t-channel (b) Wt-channel associated production (c) s-channel.

In the standard model, the top quark is assumed to decay almost exclusively into a W-boson and a b-quark. The W boson can then decay leptonically or hadronically. In the following, when discussing the analysis strategy in the s- and t-channels, we will use only the leptonic decay of the W's ($l\nu b\bar{b}$ and $l\nu b\bar{b}q$ final states, respectively)[2]. For the associated production, we will consider both cases where the leptons originates either directly from the W produced together with the top quark, or from the W-boson appearing in the top quark decay ($qq'l\nu b$ and $l\nu qq'b$ final states). The τ decay modes were included in all relevant samples, though signal selection is aimed at electron and muon signatures. Corresponding cross-sections are reported in Table 1. We note that in pp collision, the cross section for single-top is not charge symmetrical. The s-channel $t\bar{b}$ final state cross-section is thus expected to be a factor 1.6 higher than the one corresponding to the $\bar{t}b$ final state. This ratio amounts to 1.7 in the t-channel. This feature is of special interest since it generates a charge asymmetry in the leptonic final state that can be exploited in the analysis to reduce the contamination from the top quark pair production, which constitutes the main background to our signal. On the other hand, the rates for the charge-conjugate processes $W^- + t$ and $W^+ + \bar{t}$ are identical.

[1] The new Pythia default, known as “new shower” is used.

[2] The hadronic decay modes have obvious disadvantage for triggering and lack of lepton signature increases the background significantly. [11]

Significant sources of uncertainties affect the theoretical predictions of the production cross-sections. The s-channel is known with a precision of 9.9% at NLO, while the t-channel has an uncertainty of 4.8%. An uncertainty of 3% is quoted for the Wt-channel channel. Those uncertainties come from three main sources. The uncertainty in the parton luminosity, depending upon the choice of the parton density functions, is particularly important (2 to 4% for the s- and t- channels), since the b parton or the gluons are involved in the hard processes. The choice for the renormalization and factorization (μ) scales accounts for about 2 and 3% uncertainty in s- and t- channels calculations respectively. Finally, an uncertainty of $\pm$4.0 GeVin the top mass m_t results in an overall uncertainty of 2% (s-channel) and 3% (t-channel). The uncertainty in α_s enters marginally in the total error at a value below the 1% level. For the single top signal production, the AcerMC [12] ME generator was used with Pythia. Compared to TopRex [13] which was previously used in ATLAS, its t-channel generation method is based on a more physically motivated method [14] for combining LO and NLO diagrams. The contribution from NLO diagram is rather important for t-channel as gluon splitting to $b\bar{b}$ tends to be underestimated with the PS method. The s- and Wt-channel channels are generated at LO accuracy only. All three channels were generated with W bosons forced to decay leptonically (e or μ or τ). In the case of Wt-channel either the associated W or the W from top decay is forced to decay leptonically and no dileptonic events were included.

Process	Generator	Theoretical σ (pb)	Generator $\sigma \times BR$ [pb]
t-channel single top	AcerMC [14]	$246^{+9.3}_{-10.2}$ [8]	69.0
s-channel single top	AcerMC	10.65 ± 0.65 [8]	3.3
Wt-channel channel single top	AcerMC	66.5 ± 2.5 [10]	26.7
$t\bar{t}$	MC@NLO [15]	833^{+52}_{-39} [16]	461.0

Table 1: List of MC generators used for the analysis and theoretical cross sections.

2.2 Top pair production

Top pair production constitutes a dominant background to single-top events. The LHC total production cross-section is $\sigma(t\bar{t}) = 833^{+52}_{-39}\ pb$ [16], about 3 times larger than the corresponding total single top cross-section, and more than 80 times that of the s-channel. Given the single top final state topology characterized by one high P_T lepton, missing energy and jets, $t\bar{t}$ production represents a significant background in its lepton+jets decay mode, ie when one of the W's decays leptonically and the other hadronically ($t\bar{t} \rightarrow lvbjjb$), with a final state composed of two b jets, a high p_T lepton and missing energy. The "di-lepton" channel ($t\bar{t} \rightarrow lvblvb$) where a lepton is lost in acceptance also constitutes a major background. Finally, top pairs with one or both W decaying into a τ-lepton where the τ decays into an electron or a muon, may also survive the selection ("tau+jets" $t\bar{t} \rightarrow \tau vbjjb$ or "di-tau" $t\bar{t} \rightarrow \tau vb\tau vb$ channels).

Even at NLO, the theoretical uncertainty is dominated by the choice of the renormalization scale: a scale variation of $\mu/2\ to\ 2 \times \mu$ results in an uncertainty of about 100 pb. Uncertainties due to the choice of the parton density functions, α_s or m_t are much smaller and can be neglected with respect to the former. As these events constitute our main background, it will therefore be necessary to use cross-section directly from measurements on data to assess properly the contamination of our final sample.

For $t\bar{t}$ production, the MC@NLO generator [15] was used together with HERWIG. MC@NLO includes full NLO virtual corrections and properly matches the parton shower algorithm without double

counting[3]. Not all hadronic decay modes were considered since they are unlikely to fake the signals. The features of the events were validated with $t\bar{t}$ events generated by other generators including Alpgen and AcerMC as shown in [17].

2.3 W+jets production

$W/Z + jets$ events constitute a major source of background because of a cross-section several orders of magnitude above the single top production. NLO cross-sections are available for W+jets and Z+jets production in specific final states to which requirements reproducing typical LHC acceptance and energy thresholds have been applied. We use in the following the calculations from the MCFM [18] matrix element calculator, obtained with a threshold of $p_T(lepton) \geq 15$ GeV applied to the lepton originating from the W and a threshold of $p_T(jet) \geq 20$ GeV for the jets [19].

processus	BR $\times\sigma$ [pb]
$W \rightarrow l\nu$ + 0 parton	13400
$W \rightarrow l\nu$ + 1 partons	2610
$W \rightarrow l\nu$ + 2 partons	826
$W \rightarrow l\nu$ + 3 partons	239
$W \rightarrow l\nu$ + 4 partons	68
$W \rightarrow l\nu$ + 5 partons	24
Wbb + 0 parton	6.26
Wbb + 1 parton	6.87
Wbb + 2 parton	3.92
Wbb + 3 parton (incl.)	2.77

Table 2: Cross-section used for the $W + jets$ and $Wbb + jets$ samples.

The Alpgen generator with the Pythia parton shower algorithm was used for the generation of W + light jets events in this analysis. This generally shows a better agreement in the tail of the jet p_T distribution at Tevatron [20] and it is thus more suitable for our background estimation. Events with 0, 1, 2, and 3 extra partons were produced[4] as they are most likely to mimic the signal. The threshold p_T was chosen to be 15 GeVand the matching distance of ΔR=0.7 was used to identify the jets originating from the hard parton produced by ME. The Q^2 used in parton showering was the sum of the W mass and jet p_T ($M_W^2 + \sum_{jets}(p_T)^2$) as defaulted in Alpgen. The W boson was forced to decay leptonically. Note that these light jet samples do include Wc and Wcc events. b flavoured quarks can also appear in the gluon splitting occurring during the hadronization phase. In contrary Wbb MC samples do not include Wc or Wcc event. Note that this sample include Wb production in Alpgen.

Alpgen does not include NLO virtual corrections and its cross section remains at the LO level. More accurate theoretical calculations of matrix elements are available though only through a cross section calculator (not as event generator.) Thus, the MCFM [18] matrix element calculator was used to derive the K-factors to scale LO normalisation to that of NLO. The same generation requirements used in Alpgen were set in MCFM to obtain the cross section for the corresponding phase space[5]. Table 2

[3] event weight of -1 is assigned to events produced with MC@NLO. This also applies to t-channel single top generated by AcerMC due to a similar scheme used internally.

[4] Each process was produced exclusively and combined in the final analysis.

[5] In Alpgen, however, cuts are made on the p_T of the parton while MCFM runs a basic cone algorithm to build jets, to which

summarizes the cross section obtained by Alpgen, MLM matching efficiency (due to events vetoed in Alpgen matching process) and the K-factor obtained from this procedure. In addition to the above, W + heavy quark (b- or c-quarks) were generated separately to obtain better estimates of the contributions from these particular W events. Different strategy is required to reject these events as the standard method of b-tagging would not reject them. These events were generated using Alpgen as above.

2.4 Di-boson production

Di-boson events with light jets are a background to our signal due to the presence a high p_T lepton as well as b-jets in the final states. The $WZ \to l\nu b\bar{b}$ production cross-sections have been computed at the NLO level for specific final states including a high p_T lepton (electron or muon) and is found to be $\sigma \times BR = 426$ fb [21]. The $ZZ \to l^- l^+ b\bar{b}$ has a cross-section of 340 fb. The WW production, where a light jet is mistagged as a b-jet, has also to be considered. The corresponding cross-section ($WW \to l\nu jj$ $(l = e, \mu, \tau)$) is 24,500 fb. These processes were generated with Herwig with all decay modes though a filter was applied to select those events with an electron or a muon with p_T>10 GeV and $\eta < 2.8$.

2.5 QCD background

QCD multijet events contribute a background to the single top quark signal if one of the jets in the event is misidentified as an isolated lepton. The main source of QCD multijet events that enter the electron analysis is jets mis-identified as an electron. This mis-identification also leads to fake $\not{E}_T$. For muons, the main source is heavy flavor decays where the secondary muon goes wide of the jet or the jet itself is not reconstructed. Studies of this background have been done in the context of the $t\bar{t}$ analysis [22]. They show that for the $t\bar{t}$ this background is negligible. In the single top analysis the final state is similar, but contains fewer jets, meaning that the QCD multijet background is even smaller. Moreover, studies at the Tevatron have shown that this background can easily be reduced further by taking advantage of the event topology of these misidentified events [23, 24]. In contrast to signal events, QCD multijet events typically have a low-p_T lepton that is either aligned or back-to-back with $\not{E}_T$.

3 Simulation techniques, triggers and performance

3.1 Detector simulation

The single top analyses are performed with a full simulation of signal and background Monte Carlo samples. This was mostly done in the production framework for CSC [25]. One exception is the W + light jet sample. A sample with a large statistics was required for this channel and ATLFAST [26] was used to simulate these events.

In the fast simulation, the energy and momentum of the particles are convoluted with parameterized smearing functions which represent the behaviour of the detector, while in the full simulation, detailed calculations of the interactions of the particle with the detector is performed using Geant4. In single top analyses, the expected rejection rates for the main backgrounds being high, the use of the fast simulation appears mandatory. It is therefore important to compare its performance with the full simulation in order to obtain reliable estimates. Note that a thorough description of the object reconstruction performance is provided in [27]. We emphasize in the following only the part relevant for our analyses.

---

one specifies a p_T cut. After tuning, it was found that a 11.8 GeVcut on MCFM corresponds to the 15 GeVcut on parton p_T in Alpgen. This matched the cross section for all processes. The K-factor was then calculated using the same requirement to run both NLO and LO calculation. CTEQ6M was used for NLO calculation and CTEQ6L was used for LO.

3.2 Leptons, jet and missing energy reconstruction

Electrons are reconstructed using the medium selection based on a likelihood. They are reconstructed in the pseudo-rapidity range $|\eta| \leq 2.5$ with an isolation cut requiring that less than 6 GeV be present in a cone of 0.2 around the electron axis. This criterium is used to reduce the rate of jets mis-identified as electron. To account for degraded performance in the calorimeter simulation, events with electrons reconstructed in the crack region $1.37 \leq |\eta| \leq 1.52$ are removed. Note that no electron below 10 GeV is reconstructed, which has some impact on the rejection of di-lepton events in the selection.

For electrons above 20 GeV the reconstruction efficiency is $66.6 \pm 0.2\%$ and fast simulations are re-scaled appropriately to match the η and p_T dependences. The electron p_T resolution obtained with full simulation is somewhat different from the ATLFAST as shown in Fig.2. The tail at lower p_T is due to bremstrahlung in material before the calorimeter that are not properly taken into account in the fast simulation. The tail on the right is due to the photons radiated by the electron that end up close to the electron axis. Those photons are added to the electron energy cluster in the full simulation whereas they are discarded in ATLFAST, based on the truth information. Performance for all single-top processes are reported in Table 3.

Channel	Electron		Muon		Jet		MET
	Res (%)	Eff (%)	Res (%)	Eff (%)	Res (%)	Eff (%)	Res(%)
t-channel	2.01	62.1 ± 0.7	2.41	86.8 ± 0.5	7.88	96.1 ± 0.1	17.7
s-channel	2.02	54.2 ± 0.7	2.43	78.8 ± 0.5	7.81	94.4 ± 0.1	16.7
Wt-channel	1.90	66.7 ± 0.6	2.51	87.9 ± 0.4	8.15	90.4 ± 0.1	17.2
$t\bar{t}$ (ll,l+jets)	1.98	64.2 ± 0.5	2.44	86.9 ± 0.4	7.70	94.3 ± 0.1	17.7

Table 3: Resolution and reconstruction efficiency for signal ans background. Uncertainties come from Monte Carlo statistics only.

Muons are defined from the best match combination of the muon chambers and the trackers information (StacoMUON). They are reconstructed in the pseudo-rapidity range $0 \leq |\eta| \leq 2.5$ with an isolation cut requiring that less than 6 GeV be present in a cone of 0.2 around the central deposition. For muons above 20 GeV the reconstruction efficiency is 88% with a purity close to 100%. Fast simulation is rescaled globally to the same efficiency although it does not include the η and p_T dependence. The muon p_T resolution obtained with full simulation shows a reasonnable agreement with fast simulation results. Larger tail on the left can be explained by the bremstrahlung of muons.

Jets are reconstructed using a cone algorithm with $\Delta R = 0.4$. For jets above 30 GeV the reconstruction efficiency is similar in both full simulation and fast simulation and difference in the average number of high p_T jets is less than 1%. Jet resolutions are reported in Table 3.

The missing transverse energy is computed from the vector sum of all reconstructed electrons, photons, jets and muons in the event, to which are added the contributions from the clusters not associated with any objects. The missing transverse energy is affected by simplifications made in the fast simulation, resulting in an optimistic estimation in both the $\not{E}_T$ and ϕ resolutions. Fast simulation calculates $\not{E}_T$ closer to the truth value compared to the full simulation and the widths are approximately 25% smaller. A shift in the central value of about 2 GeV is also seen. No specific correction has been derived to account for the difference with the full simulation, as it is shown not to affect significantely the selection efficiencies.

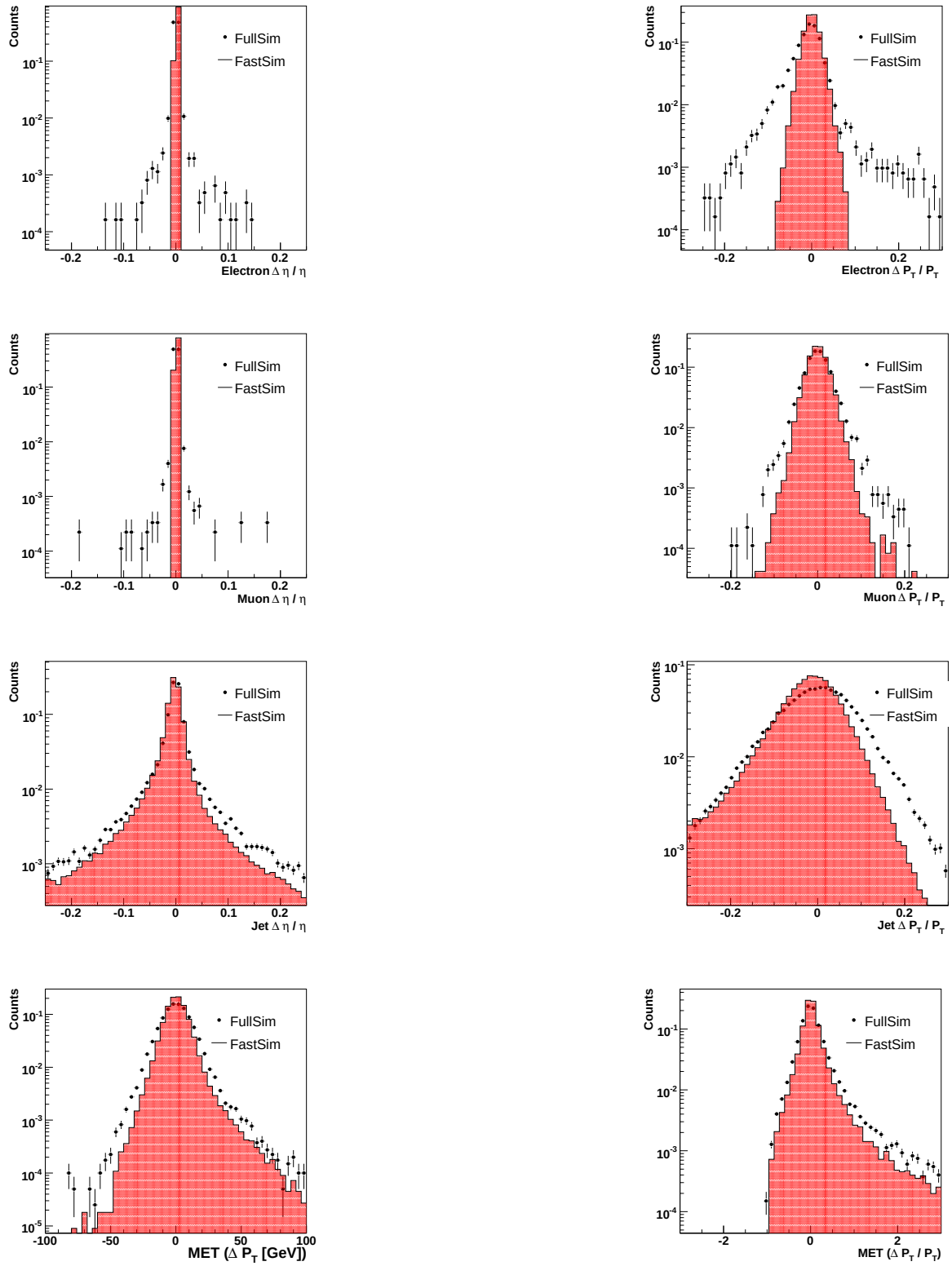

Figure 2: η and p_T resolutions for the reconstructed objects used in the analyses

3.3 Performance of b-tagging in full and fast simulation

3.3.1 Performance comparison and scaling

Since the W + light jet sample was produced with fast simulation only, we studied the b-tagging performance for full and fast simulation and obtained scaling factors for matching the performance between the two. This is described in detail in [27]. The fast simulation b-tagging is set at a constant efficiency of 60%. This neglects the p_T and η dependency of the efficiency one would observe by cutting on a likelihood weight as shown in Fig.3. Since ATLFAST has no track simulation, the likelihood weight cannot be calculated and a set of cuts were derived as a function of p_T and η for full-simulation jets to match the flat efficiency in ATLFAST. Since ATLFAST in release 12 (our main software release) was tuned to the b-tagging performance in previous release, it showed significant disagreement with the current release. This is primarily due to the increased material in the inner detector region, which degraded the rejection of the b-tagger for the same given efficiency. This can be seen in Fig. 3 and further scales were derived to reduce the fast simulation rejection to the full simulation results in the current release. Thus in this analysis, our b-taging rejection is matched to the current full simulation performance while the efficiency is taken to be 60% regardless of the jet kinematics.

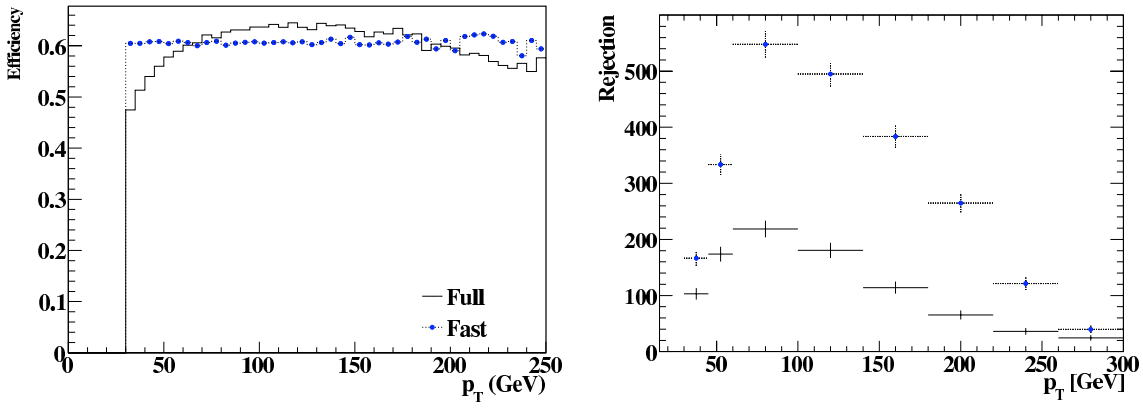

Figure 3: Full (black, solid) and fast (blue, dotted) simulation b-tagging performance. Efficiency when the overall rate is 60%(left) and rejection after matching efficiency.

3.3.2 Tagging rate function (TRF) for b-tagging

To increase the statistics for W + light jets events, an additional method was used. Most of the W + light jet events are rejected due to b-tagging requirements since the rate of light jets being tagged as b-jet is rather low. However, one can still make use of events with no b-tagged jets by assigning event weights based on the kinematics of the jets in the event. This relies on the existence of an estimation of b-tagging rejection (inverse of the probability for a light jet to be mistagged), known as "tagging rate function" parameterised as a function of the jet kinematics. A typical choice for this is the p_T and η of the jet and Fig. 4 shows such a function for light jets.

Based on this, one can examine the jet contents of the event and calculate the likelihood of the event to pass certain b-tagging requirements, such as one or more b-tagged jets in an event and make use of the events that are otherwise thrown away. Fig. 5 shows the event weights calculated for one or more b-tagged jets shown for W + light jets, $t\bar{t}$, and t-channel single top. As the efficiency of the b-tagging was assumed to be 60%, one can observe that the top events have large peak at 0.6 (one b-jet existed and it was tagged) and 84% (two b-jets existed and one was tagged) while the W + jets events mostly have lower weights due to mistagged non-b-jet.

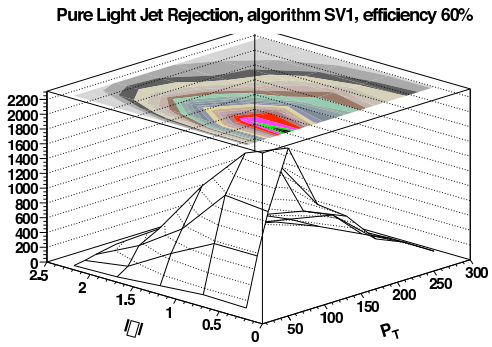

Figure 4: Rejection as a function of η and p_T for the algorithm combining SV1 and IP3D.

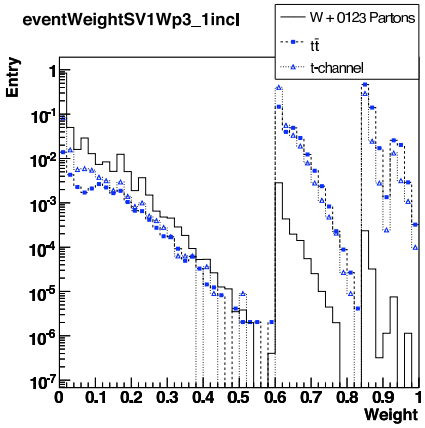

Figure 5: The event weight calculated for the event to contain one or more b-tagged jets, calculated for SV1+IP2D algorithm.

An extensive study was performed to validate and evaluate the usefulness of the method as shown in [28]. The weight calculated is used with the W + light jet events in the following analyses.

3.4 Trigger for single top events

3.4.1 Trigger definition

The final state of each single-top channel includes a single lepton and from one to three jets.[6)] Muons, electrons, and taus are produced with equal probability in W decay. Therefore, over 78% of leptonic single-top events, and all of those considered in the following analyses, include a muon or electron in the final state. Since these leptons are among the high p_T products of W decay, a relatively large lepton p_T threshold can be used to select the single-top events at the trigger level. Therefore, the most important triggers for selecting single-top events are the high p_T muon and electron triggers. Multi-jet and missing E_T triggers can be used in combination with the electron and muon triggers in order to enhance acceptance. These triggers are most important at higher luminosities but are not investigated in this report.

The three single-top channels were studied in addition to a $t\bar{t}$ sample, which included fully leptonic and semi-leptonic $t\bar{t}$ decays. The common single top event selection was applied to each sample and the electron and muon channels were studied individually. Truth and reconstructed trigger efficiencies are calculated at each trigger level. Truth efficiencies are based on the ratio of the number of truth Monte Carlo events before and after the trigger and include no event selection. This quantity gives an idea of the number of single top candidates included in the entire Monte Carlo sample. Reconstructed efficiencies were calculated using full simulation Monte Carlo events. The common single top event selection was applied before taking the ratio of the number of events before and after the trigger selection in order to calculate the efficiencies. Finally, turn-on curves are constructed using the full simulation Monte Carlo.

[6)] Only leptonic single top will be discussed in this section. Hadronic single-top, from hadronic W or tau decay, is difficult to distinguish from backgrounds and has not been studied yet.

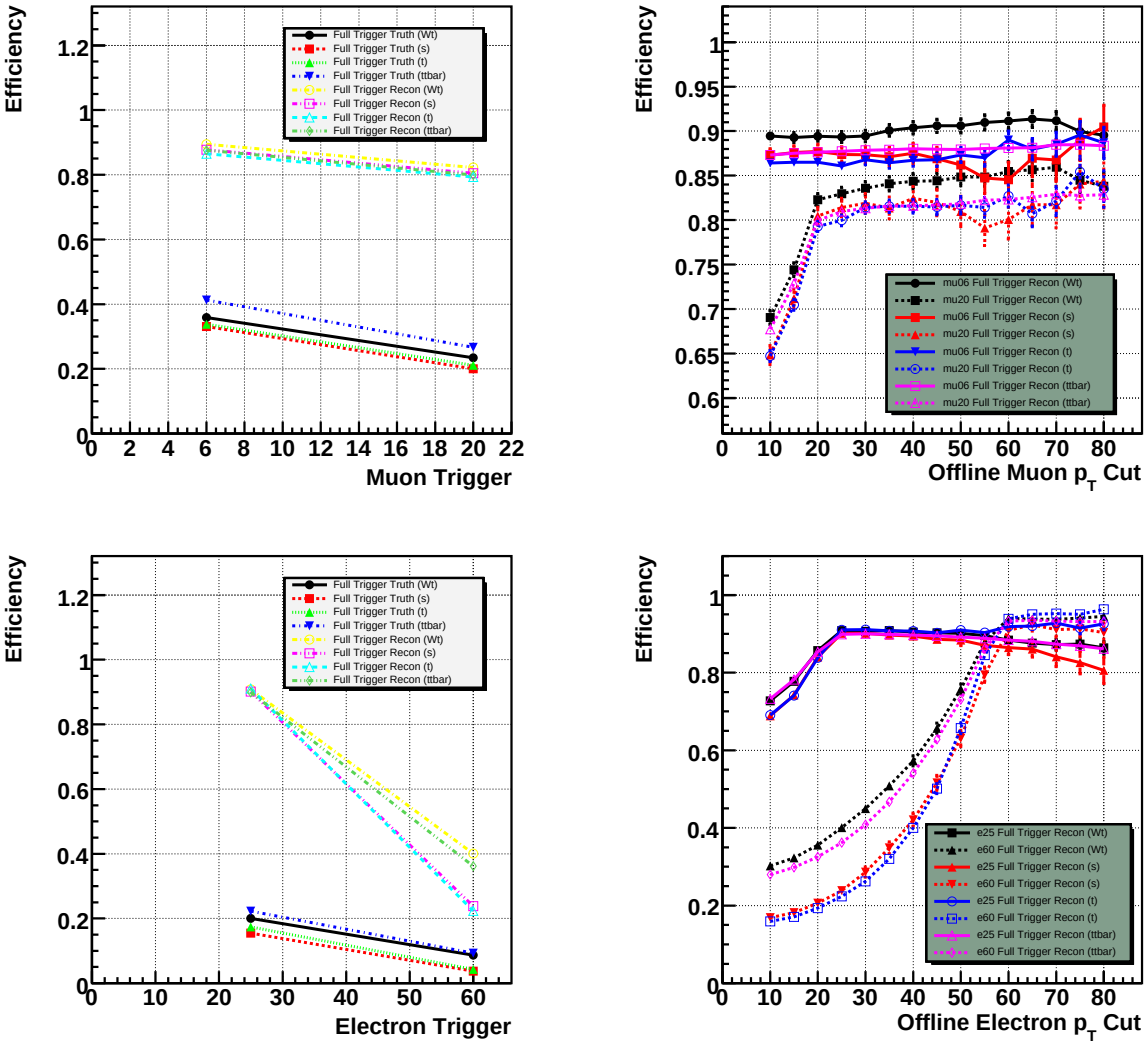

Figure 6: Effi ciencies and turn-on plots for electron and muon triggers. The upper left plot shows the muon trigger effi ciencies. The upper right plot shows the muon trigger turn-on curves. The lower left plot shows the electron trigger effi ciencies. The lower right plot shows the electron trigger turn-on curves

3.4.2 Performances

The efficiencies for the muon triggers can be seen in the upper left plot of Fig. 6. The lower set of bands show the truth efficiencies. These efficiencies are relatively low and decrease from approximately 35% for mu6 to 20% for mu20i. The truth efficiency for the $t\bar{t}$ sample is slightly higher than the three single-top samples. The reconstructed efficiencies range from approximately 90% for mu6 to 80% for mu20i and are very similar for all channels.

The turn-on curve as a function of the offline p_T cut for the muon triggers can be seen in the upper right plot of Fig. 6. The mu6 turn-on curves, represented by the solid lines, are relatively flat suggesting that the turn-on behavior occurred somewhere below the 10 GeV p_T limit imposed by muon selection.The Wt-channel channel has a slightly higher efficiency across the p_T cut range than the other three samples. The mu20 triggers, represented by the dashed lines, exhibit a turn-on behavior between 10 and 20 GeV . The different samples have similar efficiencies at low p_T cuts but at high p_T cuts the Wt-channel sample is slightly higher than the others. The proposed p_T cut of 20 GeV on muons in the common single-top event selection falls within the region of high efficiency for the mu20 trigger, although lowering this cut by even a small amount would drastically lower this efficiency.

The efficiencies for the electron triggers are shown in the lower left plot of Fig. 6. The truth efficiencies, signified by the lower set of bands, decrease from about 20% for e25i less than 10% for e60. The efficiencies for the different samples are fairly similar, although the $t\bar{t}$ and Wt-channel samples are slightly higher than the t-channel and s-channel samples. The reconstructed efficiencies, signified by the upper set of bands, show a large decrease from approximately 90% for e25i to less than 40% for e60. The efficiencies for the different samples are very similar for e25i but there is a large separation between the samples for e60. The Wt-channel and $t\bar{t}$ samples are about 40% efficient for e60 while the s-channel and t-channel samples are approximately 22% efficient.

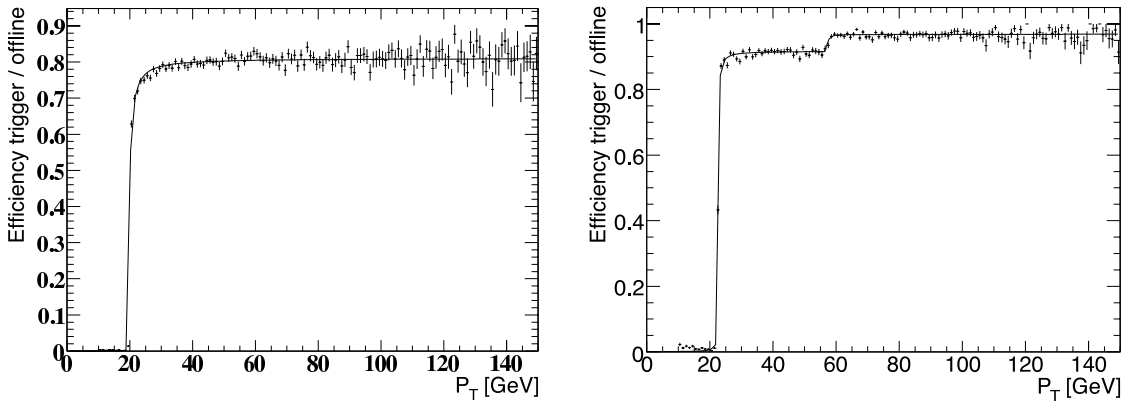

Figure 7: Muon (left) and electron (right) trigger efficiency and fit obtained from $t\bar{t}$ events. Shown for the central region of the detector.

The turn-on curve as a function of the offline p_T cut for the electron triggers can be seen in the lower right plot of Fig. 6. The e25i curves, shown by the solid lines, exhibit the turn-on behavior between 10 and 25 GeV. The different samples are similar for low p_T cuts but diverge at high p_T, with the t-channel sample increasing and the other three channels decreasing. The e60 curves, represented by the dashed lines, have a gradual turn-on between 10 and 60 GeV. At approximately 57 GeV the two sets of curves cross, with the e60 samples having a higher efficiency for high p_T cuts. This behavior is due to the isolation requirement imposed on the e25i trigger. If the logical or of e25i and e60 triggers is performed, an efficiency gain of approximately 3% can be obtained. It has therefore been decided to use the logical or of these two triggers in the common single-top event selection.

3.4.3 Trigger for ATLFAST samples

For samples processed with ATLFAST, no trigger information was available. To account for this, we used the $t\bar{t}$ sample to obtain trigger efficiency with respect to offline reconstruction as a function of p_T (fitted) and η (three bins) for both electron and muon triggers. The trigger efficiency was obtained from this based on the kinematics of the leading lepton and events were rejected using random numbers. A couple of efficiency fits are shown in Fig. 7.

4 Strategies for estimating systematic uncertainties

4.1 Introduction

During the initial low-luminosity running phase of the LHC, before single top production is fully established at ATLAS or CMS, single top production will be considered a rare process. As such, accurate estimates of signal efficiencies (and their uncertainties) are crucial to any claims of observation. The primary signatures for single top production involve single isolated leptons, several jets, and missing E_T. So, an accurate understanding of the expected jet spectra for both signal and background will be needed.

In this section we outline the method used to evaluate systematic uncertainties on the cross section measurements in the three channels as presented below. Previous studies [29, 30] identified the most significant systematic effects in top measurements. The primary concern is those arising from experimental causes including the determination of jet energy scale and performance estimation of b-tagging efficiency and rejection. Main theoretical uncertainty originate from the background normalisation and the degree of initial and final state gluon radiation (ISR/FSR). The effects of PDF and b-fragmentation parameterization had not been investigated and we present here the procedures followed to assess their impact on the selection efficiencies. Finally, the effect of the pile-up modelling is now also being considered.

4.2 Propagation and combination of errors

The measurement of the single top cross-sections is obtained with:

$$\sigma = \frac{N_{DATA} - N_{bkg}}{\varepsilon_S \times \mathscr{L}}$$

where N_{DATA} is the total number of events selected in the data, N_{bkg} the number of expected background events and ε_S the selection efficiency for signal events. As all single top cross-section measurements will be dominated by the systematic uncertainties very early, procedures have been defined in order to evaluate and, in some cases optimized, the selections in respect to the impact of the systematic uncertainties to the cross-section total error.

The propagation of the errors into the cross-section has been done in a consistent way among the three channels. The procedure generates randomly N_{DATA} according to a Poisson distribution, and makes vary randomly N_{bkg} and ε_S for every systematic source by an amount chosen around its central value, according to a gaussian distribution. This procedure is performed a few thousands times and the RMS of the resulting distribution is interpreted as the total uncertainty. The main sources of systematics taken into account are the b-tagging, jet energy scale, luminosity and uncertainties on the background level, for which central values are provided in the specific sections. Note that we consider the errors as fully correlated between signal and background for JES, b-tagging, and luminosity.

Further, this estimate has been used as a figure of merit in both the $s-$ and Wt-channel channels analyses to optimize the selection requirements: the set of cuts were chosen so that the total uncertainty as given by this procedure is minimal. The sources of systematic uncertainties and the procedures used to estimate them are described in the next Section.

4.3 Experimental systematic uncertainty

4.3.1 Jet energy scale

The determination of the jet energy scale (JES) is rather challenging in hadronic collision environment. While several methods are proposed such as using γ+jets events to propagate the electromagnetic scale to the hadronic scale, the jet energy scale depends on a variety of detector and physics effects. This includes non-linearities in the calorimeter response due, for example, to energy losses in "dead" material, and additional energy due to the underlying event. Energy lost outside the jet cone can also affect the measured jet energy. Effects due to the ISR/FSR modelling could also affect JES but they are evaluated separately below. As discussed in [31] the ultimate goal in ATLAS is to reach 1% uncertainty on JES though such performance is only reachable after several years of study. We therefore estimate the uncertainty on JES in a more realistic scenario with a preliminary calibration and so a scale variation of 5% was considered. Correspondingly, the $\not{E}_T$ was also scaled by scaling the jet contribution to $\not{E}_T$ such that

$$\not{E}'_{x(y)} = \not{E}_{x(y)} - \sum p_{x(y)} \cdot (\frac{\Delta E_{jet}}{E_{jet}}) \quad (1)$$

$$\not{E}'_T = \sqrt{\not{E}'^2_x + \not{E}'^2_y}, \quad (2)$$

where $\frac{\Delta E_{jet}}{E_{jet}}$ is +5% or -5%.

4.3.2 b-tagging

Vertex tagging of jets requires fine tuning of the inner detector performance. Determination of the b-tagging efficiency requires careful study of control samples. The effect of the uncertainty on this analysis was measured by varying the performance of b jet tagging efficiency by 5% changing the cut on b-jet likelihood. The increase in b jet efficiency is accompanied by an increased tagging efficiency of other objects, i.e. reduction of the rejection. For samples using simulated vertex information, the `weight` cut was varied so that the b-tagging efficiency shifts by this amount. For samples using parameterised b-tagging using the TRF method, the parameterisation of the b jet efficiency and c,τ,light and pure light jet rejection were varied by the corresponding amount (see section 3.3) so that the resulting tagging rates match with the likelihood cuts.

4.3.3 Beam luminosity

Luminosity determination of the proton beam is itself a challenging task. The measurement proposed in [32] is limited firstly by theoretical uncertainties such as higher-order QCD corrections, PDF and choice of scales which amounts to $\sim$ 5% uncertainty setting the limit to the determination of absolute luminosity measurement. The method is based on previously measured or precisely calculable process such as elastic proton-proton scattering [33] and QED process like $pp \to ppe^+e^-$ [34]. However, clean measurements of these processes are difficult at high luminosity phase, adding to the uncertainty of the measured luminosity. Another method suggested [35] may directly determine the parton (especially quarks) luminosity rather than proton luminosity, directly measuring theoretically uncertain quantities using Z and W boson production. Improved measurement of with uncertainty to $\sim$1% can be hoped though the method is limited by statistics in comparison to the former method.

In the first year of the LHC data taking, the expected uncertainty on the measured luminosity 20 to 30%. The integrated luminosity from this period would be up to 1 fb^{-1}. The uncertainty can be reduced to 5% level in the second year and 10 fb^{-1} of data is expected to be taken. In this year, ALFA detector is expected to refine luminosity measurement ultimately down to a few percent level. In this paper, we quote 20% uncertainty in the early data analysis and 5% in the other analyses.

4.3.4 Pile-up

At high luminosity runs above 10^{32} cm^{-2}s^{-1}, multiple hadron collision will be recorded in a given event, the effect known as "pile-up". In most cases this results in additional emission of particles due to the extra non-elastic scattering. The effect of this can be observed in jet calibration and jet multiplicities. To estimate the effect on the physics analyses caused by pile-up, a fraction of signal and $t\bar{t}$ background processes have been processed with pile-up. The overall effect on the selection efficiency can thus be estimated by comparing with our default no pile-up samples. Note that no systematic uncertainties are computed from this global factor to the analysis. We will only observe the differences caused by the addition of the pile-up to indicate that the study of high-luminosity data would require pile-up included in MC samples.

4.4 Theoretical and MonteCarlo systematic uncertainties

4.4.1 Gluon radiations

Previous single-top studies [29] have found significant uncertainties due to the modeling of the initial- (ISR) and final-state radiation (FSR). It was seen that ISR primarily affects the jet multiplicity of the event whereas uncertainties in the modeling of the FSR can affect the determination of the jet energy scale and thus the selection efficiencies. However, these initial findings were based on studies in which ISR and FSR processes were turned on or off in the simulation. As described in [36], more sophisticated treatments modify within "reasonable" expectations the values of the various parameters in the showering MC which contribute to the initial and final state radiation.

As noted in Sec. 3, the ATLAS MC generator framework makes use of the independence of the different phases of the overall collision (factorization) and allows for a two-stage procedure for event generation: in the first stage, any of a number of state-of-the-art parton-level generators (LO or NLO) may be employed to produce four-vectors of the final-state particles; in the second stage, these final-state particles are evolved with well known (and well tuned) showering algorithms found in more longstanding generators such as Pythia and HERWIG. Following the procedure for estimating ISR/FSR systematics used by the top mass group, the ISR/FSR systematic studies for single top has used as a baseline the recently developed ATLAS UE (underlying event) tune which specifies the settings of the many switches within Pythia which control essentially all free parameters in the underlying event, initial- and final-state radiation, showering, and additional hard scatters (multiple interactions). A review of these parameters identified 67 different variations of the default Pythia settings which either directly or indirectly impact the amount or nature of the initial- and/or final-state radiation. Based on the ISR/FSR studies of the top mass group, the effect of an individual variation on single top efficiencies were expected to be rather small. Therefore, large numbers of events are necessary to establish a significant effect.

It was decided to begin with AcerMC+Pythia and focus initially on s- and t-channel and perform "generator-only" level studies to identify which settings significantly shift ($> 1\%$) the selection efficiency in a positive or negative direction. These settings could then be combined into one (or more) "efficiency-increasing" choice of settings and one (or more) "efficiency-decreasing" choice of settings. Samples with these "efficiency-increasing" and "efficiency-decreasing" settings would then be run through the fast detector simulation to obtain estimates of the effect of initial- and final-state radiation on the single-top selection efficiency. It was found that the set of parameters meeting the $\Delta\varepsilon > 1\%$ requirement differed depending on the number of jets required. Further studies found that pre-selection choices with jet requirements of $N_j = 2$ and $N_j = 2\text{or}3$ corresponded to sets of parameters with such significant overlap that the sets could be combined. Likewise, preselections with jet requirements of $N_j = 3$ and $N_j = 3\text{or}4$ corresponded to sets of parameters with such significant overlap that these sets could be combined. The combined parameter sets were given the names "2jet" (for parameter settings which correspond to jet

the requirements of $N_j = 2$ and $N_j = 2\text{or}3$) and "3jet" (for parameter settings which correspond to jet the requirements of $N_j = 3$ and $N_j = 3\text{or}4$). This led to four variation sets per sample which were to be processed through ATLFAST: 2 jet-high, 2 jet-low, 3 jet-high, and 3 jet-low.

4.4.2 Background cross-sections

Currently the level of background is estimated solely from theoretical prediction. While most processes are normalised to NLO cross-section, there are still some uncertainties on the cross-section of background processes. The main source of these uncertainties are: the choice of factorisation and renormalisation scale, the choice of PDF, and the top mass. The effect of these cross sections has been studied in [8, 29, 37] and we use the values shown in table 4 as uncertainty of background cross-section. Large uncertainties in W+jet channels are particularly troublesome. The uncertainty could be reduced by measuring the cross section of these channels from data.

Process	Scale	PDF	m_t	total
t-channel (signal)	$\pm 3\%$	$^{+1.3}_{-2.2}\%$	$^{-1.46}_{+1.56}\%$	$^{+3.76}_{-4.12}\%$
s-channel	$\pm 2\%$	$^{+3.3}_{-3.9}\%$	$^{-3.94}_{+4.52}\%$	$^{+6.08}_{-6.03}\%$
Wt channel	$\pm 3\%$			$\pm 3\%$
$t\bar{t}$				$\pm 12\%$
Wbb + jets				$\pm 9.0\%$
W + jets				$\pm 15.0\%$

Table 4: Estimated theoretical uncertainties of the cross-section for the relevant processes.

4.4.3 Parton distribution functions

The distribution of longitudinal momenta of a given parton inside the colliding protons is described by a parton distribution function (PDF). The parameterization and uncertainty of the PDF affect any measurement of a physical observable, e.g. the cross-section measurement. The uncertainty on the PDF parameterization arises from the uncertainty in the global fit of hundreds of experimental data sets, and from theoretical errors in extrapolating to the event scales Q of the LHC.

The magnitude of the PDF uncertainties are expected to be small at the LHC, which can be justified qualitatively in Fig.8 where the sampled phase space (x, Q) for incoming partons in $s-$ and $t-$ channel singletop events is shown, as well as the relative uncertainty in the PDF as a function of (x, Q) for the CTEQ6.1 PDF set. One can see that the majority of the events are in regions of low PDF uncertainty.

A global fit uses a predefined parameterization of the PDF, which is a combination of parameterized quark and gluon distributions inside of a colliding particle and usually depends on many free parameters. In the so-called Hessian formalism, the gradient directions of the free parameters in the PDF global fit are transformed into an orthonormal set that completes the parameter space, such that each single parameter variation by the same $\pm t$ - value leads to the same T^2 - deviation of global fit χ^2 from the fit minimum [38] [39]. Different authors of PDF parameterizations choose different T - tolerance values. Here, we used the CTEQ6.1 PDF error set [38], where the 95% confidence level limit for the global fit χ^2 variation is used to determine T. CTEQ6.1 contains 41 member PDFs, which includes the central value PDF (evaluated with the global fit parameter values at the minimum) and 40 error PDFs corresponding to the $\pm t$ variation of each of the 20 generalized parameters of the global fit.

As mentioned, the CTEQ6.1 error sets employ the Hessian formalism for deriving PDF uncertainties.

In this model, the formulae for calculating the $\pm$ systematic uncertainty on a given measurable ε are:

$$\Delta^{+}\varepsilon = \sqrt{\sum_{i=1}^{N} \max(\varepsilon_i^{max} - \varepsilon^0, 0)^2} \tag{3}$$

$$\Delta^{-}\varepsilon = \sqrt{\sum_{i=1}^{N} \max(\varepsilon^0 - \varepsilon_i^{min}, 0)^2}. \tag{4}$$

In these equations, N is the number of global fit parameters and ε^0 is evaluated at the central value PDF. The measurables ε_i^{max} and ε_i^{min} are the maximal and minimal values of ε obtained using error PDF pair (usually called $S_i^{\pm}$) corresponding to the $\pm t$ variations of the i^{th} parameter. The general idea is to generate $2N$ datasets using each of the error PDFs, and then use Eqs. 3 and 4 to calculate the uncertainty on ε. In spite of the simplicity of the above formulae, their usage only provides correct results if the ε values are measured with a high enough statistical precision. Otherwise, a statistical fluctuation on the measurement can significantly bias the result. Using them for the calculation of the single-top selection efficiency uncertainty with statistically stable results would require the generation and simulation of tens of millions of events for each error PDF. This would demand inordinate computing power.

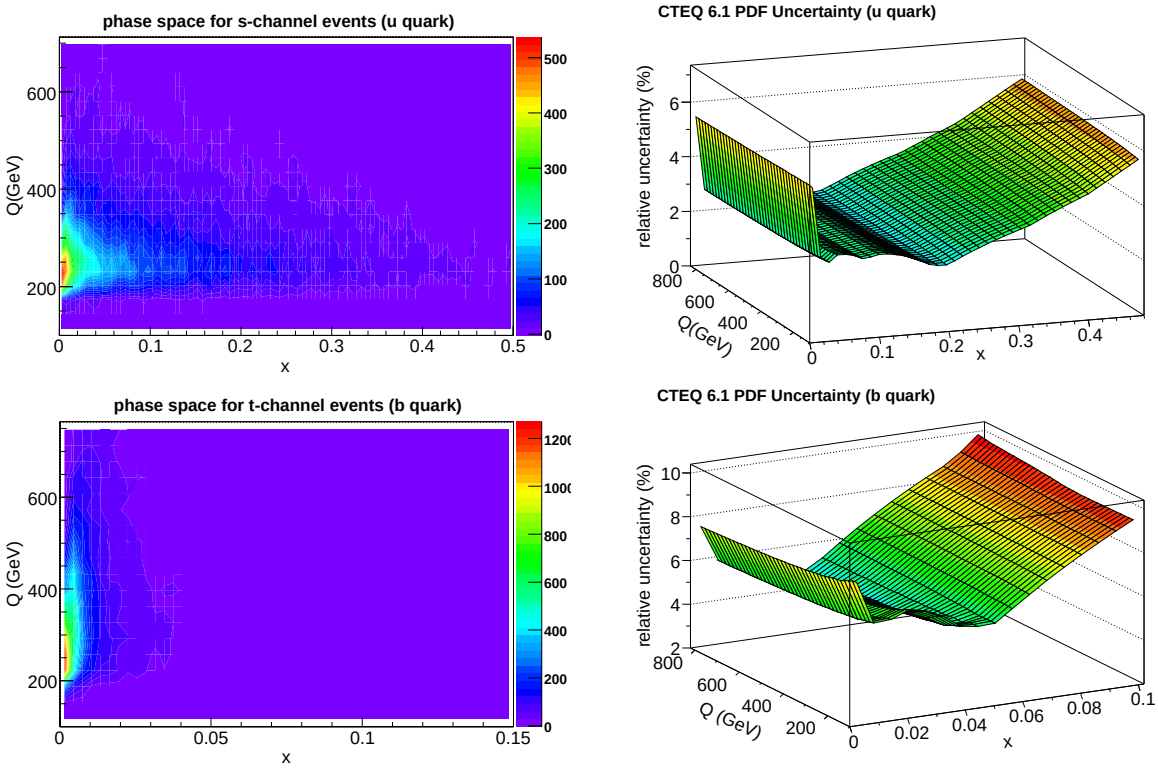

Figure 8: Sampled phase space for incoming u quarks in s-channel events (upper left plot) generated with McAtNLO 3.3. Relative uncertainty in the u quark PDF as a function of (x,Q), using the CTEQ6.1 set (upper right plot). Sampled phase space for incoming b quarks in t-channel events, generated with McAtNLO 3.3.(lower left plot). Relative uncertainty in the b quark PDF as a function of (x,Q), using the CTEQ6.1 set. (lower right plot)

An alternative way is to use a PDF re-weighting method. The event generation and reconstruction is done only for the central value PDF. For the error PDFs each event will have $2N$ weights calculated

according to this formula:

$$w_i^{\pm} = \frac{f_1(x_1, Q; S_i^{\pm}) \cdot f_2(x_2, Q; S_i^{\pm})}{f_1(x_1, Q; S_0) \cdot f_2(x_2, Q; S_0)} \tag{5}$$

Here, f_1 and f_2 are PDF values for a given hard scattering process (characterized by flavors f and momentum fractions x of the initial partons, and by Q, the event scale) evaluated for the i^{th} error PDF pair $S_i^{\pm}$. The terms in the denominator are obtained with the central value PDF and used for the event generation. For an uncertainty calculation, the events are taken into account together with the corresponding PDF weights. For example, instead of $2N$ selection efficiency values one needs to use $2N$ weighted and normalized sums of selected events as given with the formula:

$$W_i^{\pm} = \frac{\sum_{j=1}^{m} w_{ij}^{\pm}}{\sum_{k=1}^{M} w_{ik}^{\pm}} \tag{6}$$

where, M and m are total and selected numbers of single top events respectively. The $W_i^{\pm}$'s form a set of normalized $2N$ weight sums. They replace selection efficiencies $\varepsilon_i^{max} \rightarrow \max(W_i^+, W_i^-)$ and $\varepsilon_i^{min} \rightarrow \min(W_i^+, W_i^-)$ in Eqs. 3 and 4.

The benefit of the PDF re-weighting method is that it requires event generation and reconstruction only at the central value PDF and, since weighting is applied to the same events, the statistical errors on the accumulated weight sums do not affect the calculation of the systematic uncertainty. One concern with the re-weighting method is that it does not correctly account for the difference in the initial state parton evolution from differing PDFs. However, it has been shown that this is a negligible effect in most cases [40].

Note that the impacts on the selection efficiencies have been estimated using both AcerMC (interfaced with PYTHIA) and MC@NLO (interfaced with Herwig) generators. The relative PDF uncertainies from both studies are in good agreement. Since results are depending upon the full selection applied to the events, results specific to the $s-$, $t-$ and Wt-channel channels are reported in the corresponding sections.

4.4.4 b-quark fragmentation

The b-quark fragmentation determines the spectrum of the b-flavored hadron distribution as a parameterized function of the Lorenz-invariant energy-momentum variable - z [7)]. Parameterization of the b-fragmentation function is done using experimentally observed spectra of b-flavored hadrons by z. Therefore, it contains some uncertainty due to the statistical and systematic errors inherited from the used experimental data. The b-fragmentation parametrization uncertainty affects b-tagging efficiency and b-hadron energy spectrum in Monte-Carlo, which can be an additional source of single top selection efficiency systematical uncertainty.

The relevant study has been made using the already existing result [41] for the b-tagging efficiency uncertainty due to a choice of the different b-fragmentation parametrization, Peterson [42] versus Lund-Bowler [43] [44] model. According to this result the Lund-Bowler parametrization against the Peterson parametrization leads to the increase of b-tagging nominal efficiency, 0.6, by $\pm$ 0.011. This result is used for estimating the corresponding selection efficiency uncertainty using an event weighting method. The normalized weights sums for selected events were determined considering the specific selection cut requirements on b-jets in the different single top channels:

$$w_{s-channel}^{\pm} = \frac{1}{N} * \sum_{i=1}^{n} \frac{P_i^{0.6\pm0.011}(\text{exactly 2 truth b-jets out of M with } p_T > 30\text{GeV are tagged})}{P_i^{0.6}(\text{exactly 2 truth b-jets out of M with } p_T > 30\text{GeV are tagged})} \tag{7}$$

[7)] sometimes there are different non Lorenz-invariant definitions for z for experimental convenience

$$w^{\pm}_{t-channel} = \frac{1}{N} * \sum_{i=1}^{n} \frac{P_i^{0.6\pm0.011}(\text{at least 1 truth b-jet out of M with } p_T > 50\text{GeV is tagged})}{P_i^{0.6}(\text{at least 1 truth b-jet out of M with } p_T > 50\text{GeV is tagged})} \quad (8)$$

where, $P_i^{0.6}$ and $P_i^{0.6\pm0.011}$ are the binomial probabilities for i-th event calculated at the b-tagging efficiency values: 0.6, 0.611 and 0.589. M is the number of truth b-jets in the i-th event satisfying a p_T requirement. N and n are the number of total and selected events respectively. The accumulated normalized weight sums were used to calculate corresponding up and down uncertainties on the selection efficiency. This is done using the similar procedure of PDF uncertainty calculations using the formulas 3 and 4.

Since results are depending upon the full selection applied to the events, results specific to the $s-$, $t-$ and Wt-channel channels are reported in the corresponding sections. The corresponding study to estimate the influence of b-fragmentation uncertainty on the b-jet transverse momentum distribution is made with enough statistical accuracy. For this goal the Peterson b-fragmentation model with the variating free parameter - $\varepsilon_Q = 0.006 \pm 0.0025$ is used in the event generation with Pythia. Atlfast within the Atlas Release 13.0.30 is used for the event simulation.

W+jets events constitute another major source of background because of a cross section several orders of magnitude above the single top production. The LO Alpgen generator with the Herwig parton shower algorithm was used for the generation of W+jets and $Wb\bar{b}$+jets events in this analysis. A 20% uncertainty on the W+jets and $Wb\bar{b}$+jets cross-sections is considered in the following. We also studied WW and WZ diboson processes using samples generated with the Herwig generator.

5 Single top event preselection

The three production modes of single top events are characterized by similar features that lead to define a common set of preselection criteria. This preselection, which classifies the events according to exclusive electron and muon streams, is also aimed at reducing the level of three types of processes which constitute the main backgrounds to single top analyses: the top pair production, the W+jets and the QCD events.

5.1 Triggering and event preselection

The triggers for single top events rest upon the use of the inclusive isolated electron and muon triggers. Their design and performance for the three levels of trigger are presented extensively elsewhere [45]. Triggering efficiency is 84$\pm$1% overall for top quark events. Note that for fast simulation samples like W+jets datasets, where no trigger information is available, we use turn on curves derived from $t\bar{t}$ Monte Carlo samples [46].

Selected events must have at least one offline high p_T isolated lepton in the central region. The isolation criterion requires that the energy in a cone of ΔR= 0.2 around the lepton direction be less than 6 GeV and is important for the rejection of QCD background in which a jet can fake an electron or a muon [47]. Muons and electrons are required to have a transverse momentum greater than 30 GeV ensuring that the trigger efficiency is on the plateau and hence less sensitive to trigger uncertainties. Finally, the sign of the highest p_T lepton gives the flavor of the decaying top quark.

The event must then pass a second isolated lepton veto cut, applied to any lepton with a p_T above 10 GeV disregarding its sign, in order to reduce contamination from dilepton backgrounds. The rejection of $t\bar{t}$ events in the dilepton channel is increased by a factor 2.5 as this requirement is applied. The impact on the signal efficiency is limited, with a loss of 3.6% in both the s- and t-channel and 2.7% in the Wt-channel. Note that this lepton veto also ensures the orthogonality of both electron and muon selections in two exclusive streams.

Events are preselected if at least two jets with p_T above 30 GeV are reconstructed. The $t\bar{t}$ production being the dominant background to single top analyses, the use of a jet veto appears mandatory. The event jet multiplicity is required to be lower or equal to four, with the jets being reconstructed with p_T above 15 GeV. For the $t\bar{t}$ production, it is important to keep this threshold as low as possible, since lowering the veto p_T threshold from 30 to 15 GeV results in a rejection increased from 5 to almost 10. Among those events, the l+jets and the τ decay modes are the most sensitive to such a requirement with a rejection rate that is doubled compared to the 30 GeV threshold. Dilepton events are less affected with a rejection rate going from 5 to 6.6. This requirement results in a relative loss of 20 to 25% of the single top in the t- and Wt-channel channels and of 7% in the s-channel.

Among those jets, one at least must be b-tagged and have a p_T above 30 GeV . The probability for a jet to be identified as a b-jet is provided by a b-tag weight derived from the combination of two different taggers, one based on the jet tracks impact parameters and one using the secondary vertex information [48]. We select a cut on the b-tag weight corresponding to a 60% b-tagging efficiency and a mistag rate of light jets of 100 [48]. The mistag rates being high, we use an additional method to estimate backgrounds which do not contain b partons in the final states but are present in the selected sample because of a cross section several orders of magnitude above that of the signal. In those events, each jet is assigned a tag weight based on the parameterization of the mistag rate as function of the jet pseudo-rapidity and transverse momentum. The combination of all jets results in a weight assigned to the event to be considered as a "1 b-tag inclusive", "2 b-tags" etc... event. Known as the "tagging rate function", this method improves the statistics in the distributions of such events, while keeping a global normalization corresponding to the actual mistag rates [28].

Finally the transverse missing energy is required to be larger than 20 GeV. This criterion is consistent with the leptonic decays of a W boson while reducing the contamination from QCD events.

5.2 Preselection efficiency

Preselection efficiencies as well as event yield for an integrated luminosity of 1 fb^{-1} are reported for the three single-top channels, the top pair production and the W+jets backgrounds in Table 5.2. The single top efficiency ranges between 9 and 10% in the electron channel and between 10 and 12% in the muon channel respectively. These numbers translate into a total of 5,700 and 4,660 single top events in the electron and muon channel respectively.

The production of $t\bar{t}$ events constitutes the dominant source of background to single top analyses. The $t\bar{t}$ events in the $l + jets$ $(l = e, \mu)$ modes are selected with an efficiency lower than or equal to 10%, resulting in a total of 22,000 events. The $\tau + l$ (and $\tau\tau$) modes also contribute significantly with about 6,000 expected events. Despite the use of a second lepton veto, dilepton events where a lepton is lost in acceptance also contribute to the preselected sample significantly with 4,000 events surviving the selection.

The production of W+jets events is a dominant source of backgrounds, with about 13,000 events in the preselected sample. However these events populate mostly the lower jet multiplicity bin and their selection depends crucially on the mistag rates. The selection of $Wb\bar{b}$+jets events is about 2.6% resulting in about 1,000 events.

5.3 Strategy to remove QCD background

A strategy common to all single top analyses has been devoted to the rejection of the QCD events that pass the selection because of the presence of a fake lepton. This strategy has been used by the D0 collaboration [49] and is based on a feature specific to mis-measured leptons or lepton in a jet.

In the case of fake electron, the reconstructed electron candidate is shown to carry only a fraction of the initial parton energy, typically 60% [47]. This effect depends upon the location of the jet in the

process	muon channel		electron channel	
	$\varepsilon(\%)$	N(1fb^{-1})	$\varepsilon(\%)$	N(1fb^{-1})
s-channel$\rightarrow l$	7.10%	166$\pm$3	5.84%	136$\pm$3
s-channel$\rightarrow \tau$	0.68%	8$\pm$1	0.53%	6$\pm$1
t-channel$\rightarrow l$	5.89%	3143$\pm$80	5.23%	2787$\pm$76
t-channel$\rightarrow \tau$	0.63%	169$\pm$19	0.35%	92$\pm$14
Wt-channel$\rightarrow l$	6.80%	1314$\pm$27	5.64%	1091$\pm$24
Wt-channel$\rightarrow \tau$	0.96%	93$\pm$7	0.79%	77$\pm$7
$t\bar{t}\rightarrow l+jets$	4.89%	11846$\pm$130	4.44%	10734$\pm$124
$t\bar{t}\rightarrow \tau+jets$	0.63%	757$\pm$34	0.52%	625$\pm$31
$t\bar{t}\rightarrow ll$	5.84%	2257$\pm$58	4.56%	1762$\pm$51
$t\bar{t}\rightarrow l+\tau$	7.90%	3055$\pm$66	6.71%	2595$\pm$61
$t\bar{t}\rightarrow \tau\tau$	1.63%	158$\pm$16	1.57%	151$\pm$15
$Wb\bar{b}$+jets$\rightarrow l$ or τ	2.6%	514$\pm$21	5.8%	424$\pm$19
W+jets$\rightarrow l$ or τ	0.014%	7437$\pm$105	0.011%	5449$\pm$90
WW	0.32%	78$\pm$11	0.50%	65$\pm$10
WZ	0.64%	50$\pm$3	0.26%	39$\pm$3

Table 5: *Preselection efficiency, including trigger, for signal and background events. The uncertainties come from binomial error due to Monte Carlo statistics only. Note that we use the convention $l = e, \mu$.*

detector and on the reconstruction algorithm that is used to form the object. As the jet is removed from the counting procedure, the total energy imbalance of the event is modified, leading to a small fake missing transverse energy aligned with or back-to-back with the electron. A similar feature is seen with the muon, although the jet is not removed from the jet count.

The angle between the lepton and the missing transverse energy directions $\Delta\Phi(lep, \vec{\not{E}}_T)$ is represented versus $\not{E}_T$ in Figure 9. For dijet samples, the events are distributed in the region of low $\not{E}_T$ with a direction along the electron direction. This feature does not appear in top events, as seen for the t-channel, the s-channel and the $t\bar{t}$ events. From this characteristic, a "triangular cut" can be defined such that: $\Delta\Phi(lep, \vec{\not{E}}_T) > 1 - 1/80 \times \not{E}_T$. The rejection brought at the preselection stage is about 250 for dijets in the [30-140] GeV and about 85 in [140-280] GeV energy ranges. The corresponding loss of efficiency in the single top channels is 4 to 5% for the s- and t-channels, and 6% to 7% for the Wt-channel and $t\bar{t}$ events.

From this procedure, it is obvious that a tuning of this requirement will be required from the data itself. This method will also need specific studies devoted to the sensitivity of the reconstruction algorithm used to form electrons and jets. In the s-channel and Wt-channel analyses, we apply this criterion to all samples and will assume that the remaining level of QCD contamination can be removed, or at least estimated, from the data itself.

Note that the use of a tight definition for the electron also brings another improvement. Requiring all electrons to be selected with the tight quality further reduces the QCD contamination by 30%. However, the corresponding loss in signal events is about 12% and such requirement has not been used in the following analyses.

Eventually, the QCD background contamination in selected samples can be monitored by the reconstruction of quantities like the transverse W boson or top reconstructed masses. The advantage of using the transverse W boson mass is that this quantity is less sensitive to a jet energy scale bias. Figure 10 shows the variable m_T^W reconstructed in the case of the Wt-channel selection without the application of

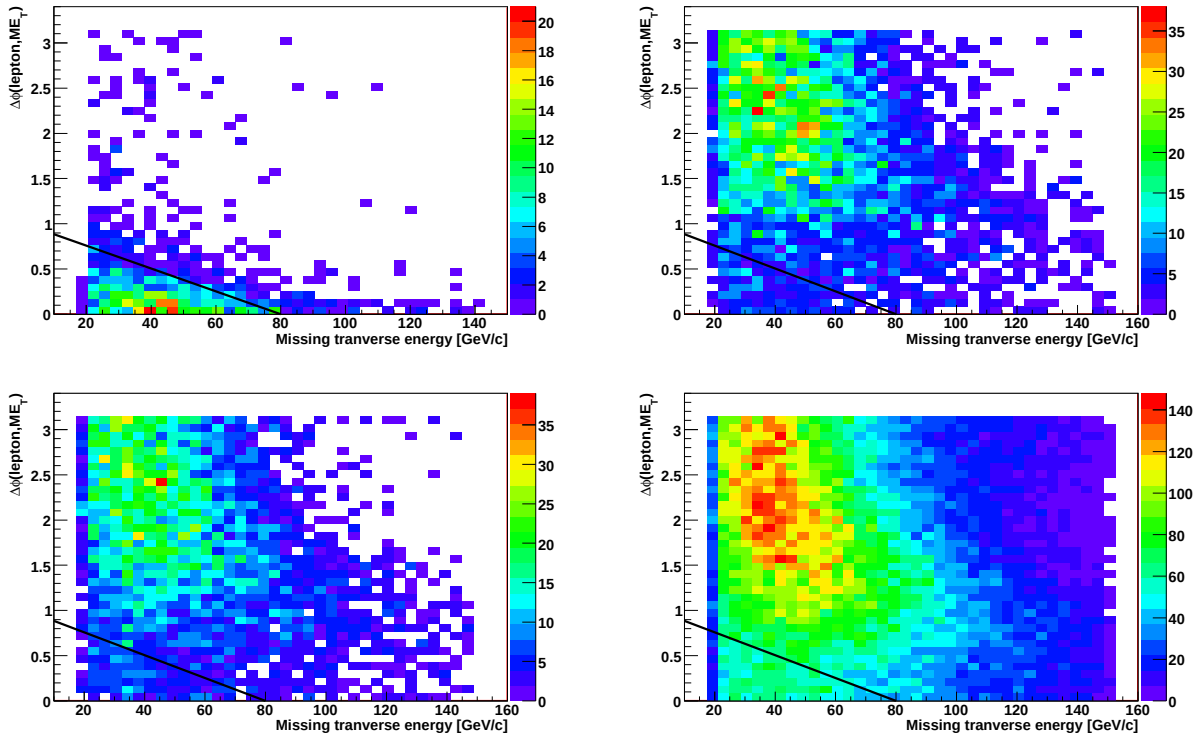

Figure 9: Triangular cuts shown in the $(\Delta\Phi(e,\not\!\!E_T),\not\!\!E_T)$ plane for dijet events (top left), t-channel events (top right), s-channel events (bottom left) and top pair lepton+jet events (bottom right).

the triangular cut. Figure 11 shows this same variable after the application of such a cut. By using the distribution in the region lower than 50 GeV, one can normalize the level of remaining background and assess the expected level in the signal region above 50 GeV, thus allowing to test the tools developed for the QCD estimation.

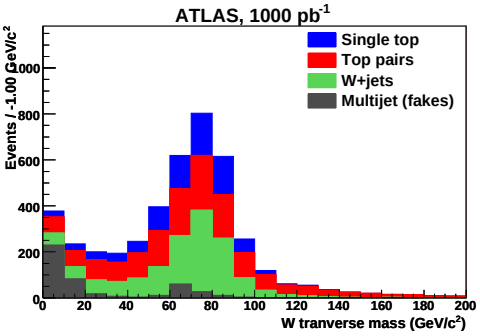

Figure 10: Transverse W boson mass after the Wt-channel selection in the case no triangular cut is applied

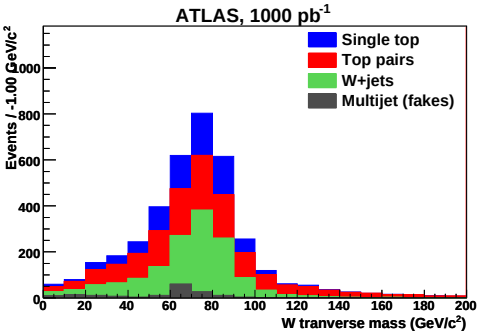

Figure 11: Transverse W boson mass after the Wt-channel selection in the case where the triangular cut is applied

6 Measurement of the t-channel cross section

The t-channel is the most promising channel for single top observation at the LHC. It has the largest theoretical cross section of the three channels[8)] and its event features give us reasonable visibility of the signal according to the studies done so far [50]. In addition to the cross section measurement, the t-channel single top is one of very few candidate channels for the $|V_{tb}|$ and the top polarization measurements. It is hoped that these measurements will shed light on our understanding of the electroweak symmetry breaking since these quantities have not been studied with high precision in past experiments. Compared to $t\bar{t}$, the t-channel single top suffers from a higher level of background due to its lower jet multiplicity. While the signal production rate is not statistically limited at the LHC, a good strategy for signal extraction is required and a careful estimation of the background rate is necessary.

The current analyses conducted at D0 and CDF have reported 3σ evidence for combined t-channel and s-channel observation, making extensive use of multivariate discrimination techniques as explained in Sec.1. At the Tevatron, the single top production cross-section is minute and the analysis is largely limited by statistical uncertainties, unlike at the LHC. In this section, we first focus on an event selection using a set of simple kinematic cuts. Such an analysis will be preferable at earlier stages of the experiment since it is easier to understand its details. However, the following study reveals that a cut-based analysis results in a large overall uncertainty due to the overwhelming background from $t\bar{t}$. Further purification of the signal is studied using multivariate techniques and possible improvements were estimated.

6.1 Cut based event selection

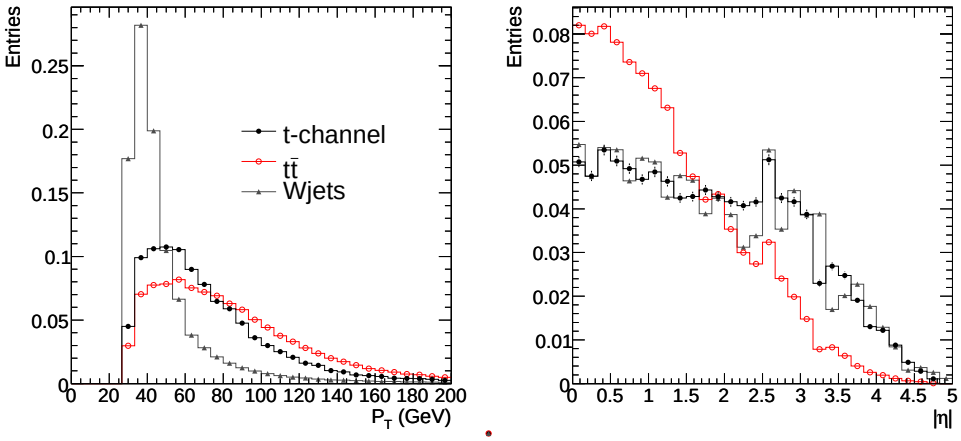

Figure 12: Signal and background distribution of the b-tagged jet p_T and non-b-tagged jet η.

After the common preselection, the contribution from the background is still high mainly due to W+jets at the lower end of the kinematic distributions (such as in the jet p_T spectrum) and $t\bar{t}$ at the higher end. The b-tagged jets coming from $t\bar{t}$ and the t-channel single top tend to have high p_T and to be located more centrally since they mainly originate from top decays. On the other hand, b-tagged jets from W events are much softer as they primarily come from mistagged jets originating from extra gluon radiations. Furthermore, the recoiling forward quark in t-channel single top produces a high p_T light jet in the forward direction. This was found to be one of few features useful to reject $t\bar{t}$ background events because light jets from the $t\bar{t}$ events are typically initiated from hadronic W decays and are therefore more central. A cut on b-tagged jet $p_T > 50$ GeV reduces the W+jets significantly, while a cut on the

[8)] About 250 pb at NLO, 15 events will be produced every minutes at the initial LHC luminosity.

hardest light jet $|\eta| > 2.5$ can reject $t\bar{t}$. Figure 12 shows the p_T distribution of the hardest b-tagged jet and the composition of the sample in terms of the jet multiplicity after the additional event selection.

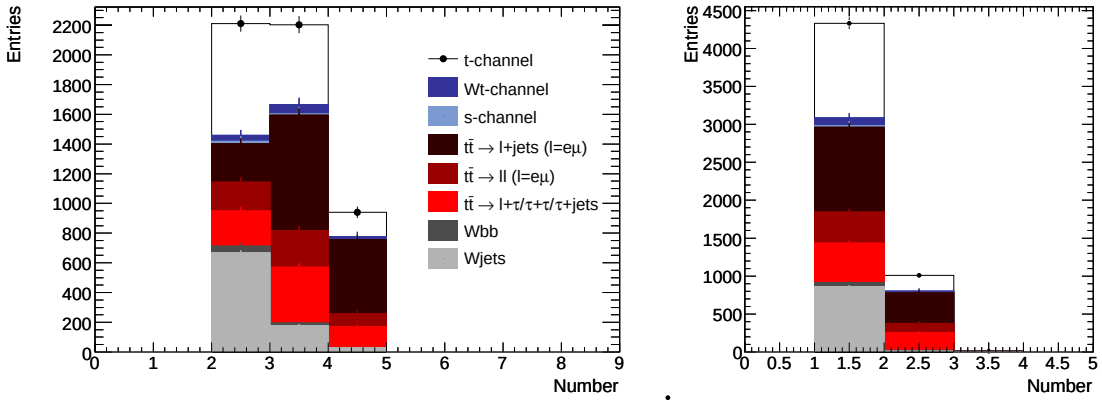

Figure 13: Multiplicity of jets with $p_T > 30$ GeV (left), and B-tagged Jets with $p_T > 30$ GeV after the t-channel final described in the text.

Table 6 lists the number of preselected events, the number of events selected after the cut on b-tagged jet p_T and the number after the light jet η cut for the signal and the background processes. Note that the signal efficiency is 1.81% and signal to background ratio after all selection is 37%. By far the largest background contribution comes from the $t\bar{t}$ process; the lepton + jets $t\bar{t}$ events contribute the most, although dilepton events have a higher survival probability of 1.36% compared to 0.64% of the lepton + jets. W+jets is the next largest background while the $Wb\bar{b}$ contribution is relatively small. The s-channel single top contribution is almost negligible and the diboson background is even smaller and therefore is not included in the table.

process	Preselected		b Jet p_T		light jet η	
	$\varepsilon(\%)$	N(1fb^{-1})	$\varepsilon(\%)$	N(1fb^{-1})	$\varepsilon(\%)$	N(1fb^{-1})
t-channel	7.7%	6191±112	5.5%	4412±95	1.8%	1460±56
μ channel	4.1%	3312±83	2.9%	2352±71	0.9%	728±40
e channel	3.6%	2879±78	2.6%	2060±66	0.9%	732±40
s-channel	9.0%	316±5	7.0%	245±4	0.8%	26±1
Wt-channel	8.9%	2575±37	6.4%	1854±32	0.4%	122±9
$t\bar{t}$ l+jets $(l = e\mu)$	9.3%	22580±176	7.3%	17775±158	0.6%	1556±48
$t\bar{t} \to l + \tau/\tau + \tau/\tau$+jets	4.3%	7342±104	3.4%	5776±93	0.4%	740±34
$t\bar{t} \to ll(l = e\mu)$	10.4%	4018±75	8.1%	3143±67	1.3%	520±28
W+jets	0.025%	12886±138	0.012%	6082±95	0.0017%	873±36
$Wb\bar{b}$	4.7%	939±27	3.0%	597±22	0.4%	69±8
S/B		0.12		0.12		0.37
$S/\sqrt{B}\,(\sigma)$		27.5		23.4		23.4
$\sqrt{S+B}/S$		3.9%		4.5%		5.0%

Table 6: *Number of events selected after each cut in the t-channel analysis. The last column shows the number of remaining events in the cut-based analysis at the integrated luminosity of 1 fb^{-1}.*

As seen in Table 6, a precision ($\sqrt{S+B}/S$) of 5% can be obtained after the final selection. Note, however, that the selection cut does not optimize the precision nor the significance of the signal observation. As it turns out, the uncertainty from systematic effects is much larger than the statistical error.

From purely statistical arguments, the t-channel cross section can be measured to a few percent accuracy with a few fb^{-1} of data.

In comparison to the previous study in the ATLAS physics TDR [50], which reported S/B ratio of 3, there is a significant reduction in event selection performance. The cut-based selection used here is similar to that used in the TDR and we would have expected a similar result. Further investigation revealed several issues with the TDR analysis. Firstly, MC generators changed drastically in recent years. Pythia introduced a new parton shower algorithm, which is much more radiative. The Matrix-Element generator for the signal has also changed to AcerMC, which combines the NLO diagram contribution to the LO ones as opposed to Pythia, which only uses LO. For the W+jets background production, Alpgen is favored at Tevatron because it produces the high p_T tails of jet distributions much more accurately than Herwig on its own, which was used in the TDR. In addition, the TDR analysis did not include some of the crucial background processes; the dilepton $t\bar{t}$ channels and all τ decay modes of signal and background were neglected although it has been shown in this analysis that these channels contribute significantly. Therefore, the result of the TDR can now be seen as too optimistic. Note that the presence of pile-up affects the reconstruction of the objects selected in the event. In particular, the selection efficiency is directly affected by the presence of extra jets in the events. Specific Monte Carlo samples of single top and $t\bar{t}$ events have been produced with or without pile-up events superimposed. The use of events with pile-up results in a decrease of about 25% for signal events, and 34% for $t\bar{t}$ events. No systematic uncertainties will be associated to this value. The use of data will be mandatory for the tuning of the pile-up modeling and the corresponding uncertainty is expected to be brought down to a negligible value with respect to the other sources of error.

6.2 Systematic uncertainties

6.2.1 Experimental systematic uncertainties

process	b-tag -5%	b-tag +5%	JES -5%	JES +5%
t-channel	-3.98%	+4.77%	-4.77%	+5.04%
s-channel	-5.23%	+3.58%	-6.61%	+12.67%
Wt-channel	-8.87%	+8.87%	-1.97%	+6.90%
$t\bar{t}$	-6.40%	+6.80%	-3.06%	+5.92%
$Wb\bar{b}$	-3.98%	+8.91%	-12.62%	+12.69%
W+jets	-1.65%	+2.50%	-9.91%	+14.59%
Total bkgd.	-4.62%	+6.02%	-4.84%	+8.11%

Table 7: *Effect of b-tag and JES systematics. Numbers are quoted from relative variation of selected event.*

While the statistical uncertainty is not a constraint for the t-channel cross section analysis even with the early data, systematic uncertainties can only be reduced with detailed understanding of the detector performance and theoretical uncertainties. The measurement in the t-channel is largely limited by such effects. Various criteria need to be considered to assess the systematic effects in the t-channel measurement as it depends on a number of detector sub-components and theoretical assumptions.

Uncertainty in the b-tagging performance and the jet energy scale can have crucial effects on the measured cross section since we rely on jet kinematics to reduce the background. In particular, the large background contribution from $t\bar{t}$ can cause a large fluctuation on the total event rate with these uncertainties, which leads to a large error on the cross section measured. The jet energy scale uncertainty affects the p_T distribution of jets strongly at the low end of the distribution. Cutting on p_T in this region

can lead to a larger uncertainty on the signal acceptance. The effect of 5% variation of the b-tagging performance and the JES is summarized in Table 7. It should be noted that $Wb\bar{b}$ and W+jets are affected more by the jet energy scale due to the fact that most of the jets in these sample are in the low-p_T region, which is more sensitive to the JES variations.

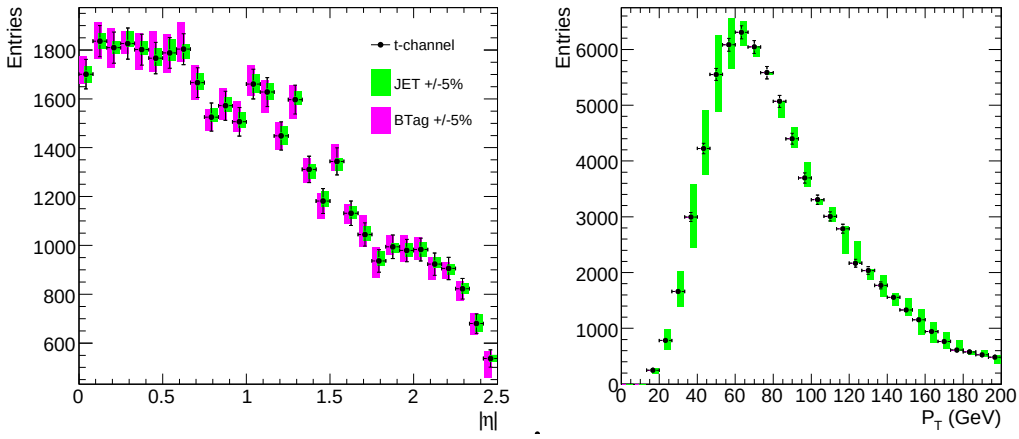

Figure 14: *The p_T distribution of the hardest jet before selection cuts. The green bars show the effect of 5% jet energy scale variation*

6.2.2 Theoretical and Monte Carlo systematic uncertainties

Since the event selection relies heavily on the jet multiplicity, the number of additional jets from the parton shower can affect the selection efficiency. To evaluate the effect of ISR/FSR uncertainty, two sets of Pythia parameter variations were considered for comparison, which control free parameters in the underlying event, initial- and final-state radiation, showering, and multiple interactions. The variations were combined to maximize the variation of event selection to give a conservative estimation. The effect on the jet multiplicity is shown in Figure 15. It can be seen that the loose jet distribution is affected more severely, which affects the selection efficiency due to the jet veto cut. The overall uncertainty in t-channel selection of -10.6% $+7.2\%$ was seen from the parameter variation set that gave a larger uncertainty.

The uncertainty on the t-channel cut selection efficiency due to PDF is summarized in Table 8. The numbers were estimated at generator level using a similar selection cuts to this analysis. The effect of the PDF uncertainty on the signal was evaluated to be +1.38% -1.07% by taking the average of electron and the muon channel and it is a minor contribution to the final systematics. A larger effect of +6.2% -5.45% was seen on the $t\bar{t}$ background.

Channel / Final State	$\varepsilon \pm \Delta\varepsilon$(stat.)%	$\Delta^+\varepsilon$ / ε %	$\Delta^-\varepsilon$ / ε %
t-channel / $e^{\pm}$	5.62 ± 0.10	1.3	0.9
$t\bar{t}$/t-channel/ $e^{\pm}$	0.291 ± 0.009	6.0	5.5
t-channel / $\mu^{\pm}$	6.44 ± 0.11	1.4	1.1
$t\bar{t}$/t-channel/ $\mu^{\pm}$	0.313 ± 0.009	6.4	5.4

Table 8: The uncertainty on selection efficiency due to PDF, evaluated using the PDF error sets from MRST and CTEQ as described in Section 4.4.3

In addition to the above, the t-channel process has a fairly large uncertainty from MC generator predictions. Comparing various combinations of ME and PS generators, it was observed that the Pythia and Herwig parton shower algorithms give considerably different jet multiplicities. While we assume

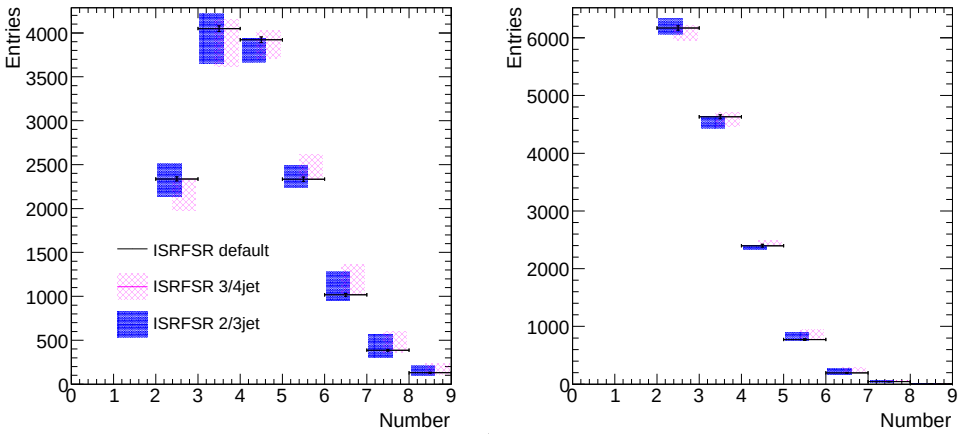

Figure 15: *Variation in t-channel multiplicity for the loose ($p_T > 15$ GeV, left) and the tight ($p_T > 30$ GeV, right) jets due to ISR/FSR parameter variation. The distributions are shown without applying the t-channel selection cuts. The jet veto cut ($\leq$ 4 loose jets) and the requirement of b-tagged jet were also removed for these plots. Black points are the nominal entries while the pink, mesh band shows variation from "3/4 jet parameter set" and the blue, fill shows that of "2/3", which are the two sets of parameter variations compared.*

that this difference can be eliminated by tuning the parameters to the observed data[9)], the instability of theoretical prediction from matrix element generators is an outstanding issue and a 4.2% variation in signal acceptance was seen by comparing AcerMC+Herwig and MC@NLO+Herwig. We quote this as an estimate for systematic uncertainty from the theoretical prediction.

In our present analysis, the background is estimated from MC and its normalization is currently estimated based on theoretical uncertainties. When data will be available, the $t\bar{t}$ and the W+jets backgrounds will be measured from data as well. It is beyond the scope of this paper to discuss methods for the data-driven background estimation and the uncertainty from the background is currently estimated based on theoretical uncertainties.

6.2.3 Summary of uncertainties

The effect of the uncertainties on the measured cross section is summarized in Table 9. We used the following expression to calculate the cross section, σ:

$$\sigma_{t-channel} = \frac{N_{sig}}{a \times \mathscr{L}} = \frac{N_{tot} - B}{a \times \mathscr{L}}, \tag{9}$$

where N_{sig} and N_{tot} are the number of signal and all selected events respectively, B is the number of background events, a is the signal acceptance and $\mathscr{L}$ is the luminosity of the data sample. The effect of each source of uncertainty on these variables is indicated in Table 9. They were combined and propagated to the measured cross section using a toy Monte Carlo method, which randomly generates N_{tot} according to a Poisson distribution, and makes vary randomly B and a for every systematic source by an amount chosen around its central value, according to a gaussian distribution. This procedure is performed a few thousands times and the RMS of the resulting distribution is interpreted as the total uncertainty.

A large part of final uncertainty is due to the overwhelming amount of $t\bar{t}$ background. For this reason, the event selection optimized for statistical significance or statistical precision does not give the smallest total uncertainty when systematics are included. The total uncertainty is dominated by systematic effects affecting the background normalization. Reducing the background contamination to increase S/B would

[9)] The current tuning of Pythia and Herwig parton shower was obtained independently based on extrapolation from the Tevatron data.

help to minimize the systematic uncertainty. It is therefore desirable to further optimize the selection beyond what can be achieved with straight cuts on the existing variables.

Source	Analysis in 1 fb^{-1}			Analysis in 10 fb^{-1}		
	Variation	Cut-based	BDT	Variation	Cut-based	BDT
Data Statistics		5.0%	5.7 %		1.6%	1.8 %
MC Statistics		6.5 %	7.9%		2.0 %	2.5%
Luminosity	5%	18.3 %	8.8%	3%	10.9 %	5.2%
b-tagging	5%	18.1 %	6.6%	3%	10.9%	3.9%
JES	5%	21.6%	9.9%	1%	4.4 %	2.0%
Lepton ID	0.4%	1.5 %	0.7%	0.2%	0.6 %	0.3%
Trigger	1.0%	1.7 %	1.7%	1.0%	3.6 %	1.7%
Cross section		22.9%	8.2%		6.9 %	2.5%
ISR/FSR	+7.2 -10.6%	9.8 %	9.4%	+2.2 -3.2%	2.7 %	2.5%
PDF	+1.38 -1.07%	12.3 %	3.2%	+1.38 -1.07%	12.3 %	3.2%
MC Model	4.2%	4.2 %	4.2%	4.2%	4.2 %	4.2%
Total		44.7 %	22.4%		22.4 %	10.0%

Table 9: *Summary of all uncertainties that affect the measured cross section, shown for the cut-based analysis and the BDT analysis. Data statistics is the poisson error one would expect from real data while MC Statistics is the uncertainty on the estimated quantities due to MC statistics.*

6.3 Multivariate event selection

In the cut-based analysis no variable was found that was effective to reject the $t\bar{t}$ background. One commonly employed separation technique is the Multivariate Analysis (MVA), which effectively factorizes the process of cut optimization using a set of rules for separating the signal from the background events. Here we attempt to eliminate the remaining background contribution from $t\bar{t}$ using the Boosted Decision Tree (BDT) method.

With the sample after the b-tagged jet p_T cut in the t-channel selection[10], 40 object/event level variables were studied using a genetic algorithm, which scanned a large number of variable sets. The figure of merit used to assess the performance of the variable combinations is their signal to background separation:

$$\frac{1}{2}\int_{-\infty}^{\infty}\frac{(s(x)-b(x))^2}{s(x)+b(x)}dx, \tag{10}$$

where $s(x)$ and $b(x)$ are the distributions given as output of the MVA for the signal and background respectively.[11] The algorithm was written in such a way to evolve the variable combinations and obtain better performance iteratively. Generations of variable sets were produced and genetically evolved to

[10] This means that the light jet η cut was removed for this study. This cut is effective to reduce $t\bar{t}$, but not very efficient and the MVA provides a more powerful alternative.

[11] This quantity has the property of being 0 for completely overlapping distributions and 1 for completely non-overlapping ones [51].

search for a large number of combinations. We then reduced the sets that contained variables that are highly sensitive to JES systematics.

It turned out that a good signal over background separation is achievable with a small subset of the variables, namely:

p_T of the leading jet	p_T of the leading non-b-tagged jet
η of the leading non-b-tagged jet	$\cos(\theta)$ of leading jet in event frame
Centrality ($\frac{p_T^{jet0}+p_T^{jet1}}{\lvert p\rvert^{jet0}+\lvert p\rvert^{jet1}}$)	Scalar sum of p_T of the two leading jets, $\not{E}_T$, and lepton
ΔR between two leading jets	ΔR between leading jet and lepton
ΔR between leading non-b-tagged jet and lepton	W transverse mass
η of jet with largest eta	Number of jets with $p_T > 30$ GeV

The distribution of these variables for the signal and the $t\bar{t}$ background is shown in Fig.16.

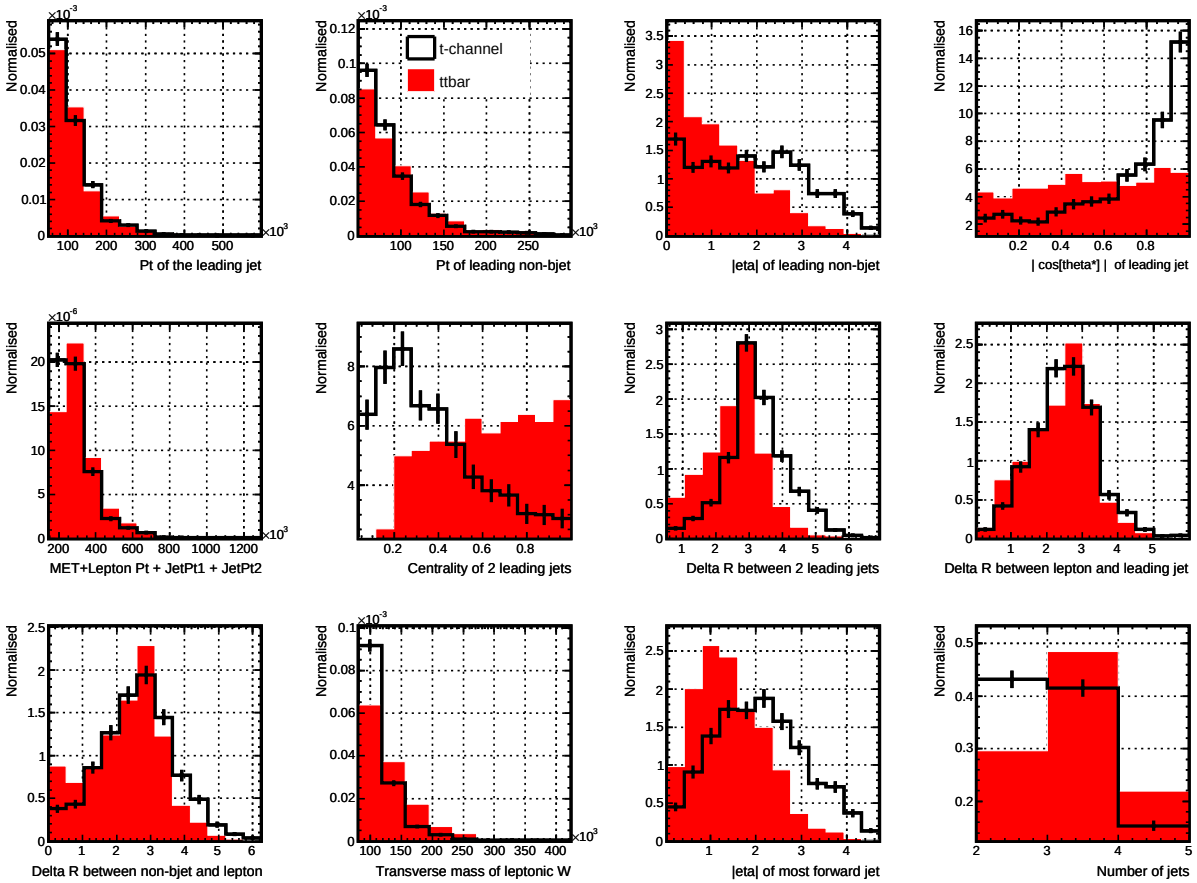

Figure 16: Distributions of input parameters for signal (solid line) and background (filled).

Figure 17 (left) shows the BDT output discriminator constructed from the variables discussed above. By cutting on a high value of the discriminator, the $t\bar{t}$ background can be removed more effectively than by cutting on individual input variables. Since the BDT was optimized for the $t\bar{t}$ separation, as expected the output is not effective against W+jets. It can be seen in the right figure that a high level of signal purification is achieved using the BDT discriminator. We optimized the cut on the BDT output

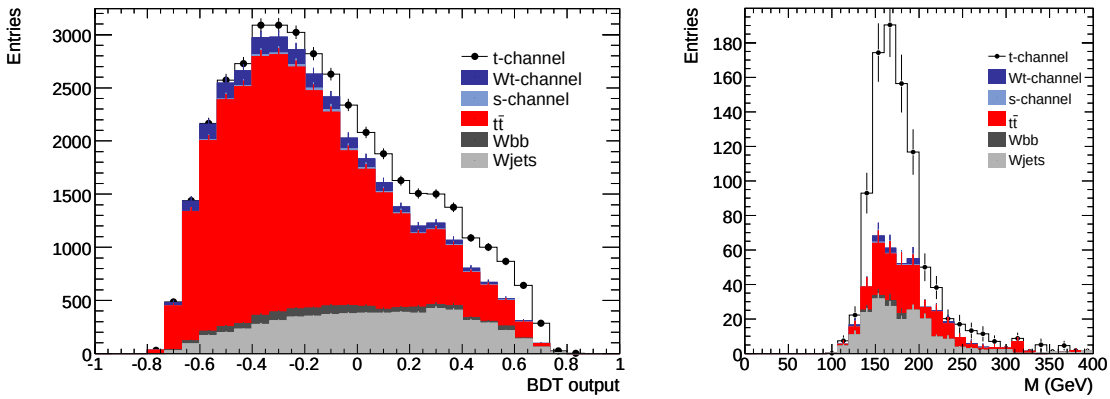

Figure 17: *Boosted decision tree output for signal and background after the b-tagged jet p_T cut (left) and leptonic top mass distribution using cut on BDT output at 0.60 (right).*

by minimizing the final uncertainty on the measured cross section, including the systematic effects. For each cut, the systematic uncertainties were calculated assuming that the relative systematic uncertainty stays constant for each channel for each source of uncertainty. This is a fairly reasonable assumption considering that the relative uncertainty changes slowly with the cuts and the variables were chosen to avoid larger systematics[12)]. For most cut choices, the systematic effects are dominant and the total uncertainty is reduced with increasing S/B ratio. On the other hand, with very tight cuts the statistical error becomes larger than systematics. The overall minimum was found to be at 0.6 where the S/B ratio is 1.3 and 542 signal events are left. The statistical uncertainty is 5.7% while the total uncertainty is 22.4%.

6.4 Sensitivity at 1 fb^{-1} and the measurement of $|V_{tb}|$

Although the estimated systematic uncertainty of the cut-based analysis is rather large (44.7%), it has been shown that this can be reduced by rejecting the $t\bar{t}$ background using boosted decision trees. The total uncertainty decreases as the S/B ratio increases and the estimated uncertainty at 1 fb^{-1} is

$$\frac{\Delta\sigma}{\sigma} = \pm 5.7\%_{stat} \pm 21.7\%_{sys} = \pm 22.4\%. \tag{11}$$

The t-channel cross section is proportional to $|f_L V_{tb}|^2$, where the parameter f_L is the weak left-handed coupling and $f_L = 1$ in the SM. In the theory predictions, the product $|f_L V_{tb}|^2$ is always set to unity. Thus, if one measures the cross section, and then divides by the theoretical cross section, one obtains a measurement of $|V_{tb}|^2$, making the SM assumption that $f_L = 1$ [52].

The relative uncertainty on $|V_{tb}|$ is the relative uncertainty on $|V_{tb}|^2$ divided by two since $d|V_{tb}|/|V_{tb}| = d|V_{tb}|^2/2|V_{tb}|^2$. However, there are additional systematic uncertainties in the $|V_{tb}|$ measurement due to the presence of the theoretical cross section in the denominator. Here, we quote the uncertainty calculated in [8], in which a theoretical uncertainty of $+3.76\ -4.12\%$ is reported including the contributions due to strong scale, PDF and top mass uncertainties. We use the average of the positive and the negative uncertainties. Therefore, the estimated uncertainty on the measured value of $|V_{tb}|$ is

$$\frac{\Delta|V_{tb}|}{|V_{tb}|} = \pm 11.2\%_{stat+sys} \pm 3.9\%_{theo} = \pm 11.9\%. \tag{12}$$

[12)] More vigorous calculation of systematics for each cut on BDT should be done in our future studies.

6.5 Summary

The cross section measurement of the single top t-channel was studied in this chapter. The characteristics of the signal and background were investigated in detail and an analysis strategy was developed first using simple cuts and then using boosted decision trees.

While a cut-based event selection can achieve a statistical precision of a few percent at an integrated luminosity of 1 fb^{-1}, the $t\bar{t}$ background is difficult to reduce. This results in large systematic uncertainties coming from both experimental and theoretical origins. Uncertainties in JES, b-tagging and luminosity all affect the measurement considerably. The uncertainty on background cross section is also rather large though we expect that it will be constrained at higher accuracy with the data. This is also true for the QCD background, which is not included in our current analysis. Data-driven background estimation methods should be developed in time for the arrival of real data. Among the theoretical issues, the ISR/FSR uncertainty degrades the measurement more significantly than other theoretical effects such as the PDF and the Monte Carlo generator model.

A multivariate background discrimination method is very effective in reducing the background and thus reducing the total uncertainty to nearly a half of the cut-based analysis. We conclude that multivariate analysis tools are highly effective for a t-channel cross section measurement and further studies of these techniques will be very beneficial for the improvement of the analysis in the future. However, to reach a precision at a few percent level, thorough studies of systematic uncertainties and an excellent understanding of the detector response will be necessary.

7 Measurement of the s-channel cross section

The measurement of the single top s-channel appears as the most delicate of the three main single-top processes. Suffering from a low cross section compared to the main backgrounds, the event final state and topology make this channel very sensitive to the presence of both $t\bar{t}$ and W+jets events. Because of the low jet multiplicity of such events, the analysis is also expected to be sensitive to dijet production, despite the tight requirements on the presence of at least two b jets. The s-channel is however one of the most interesting because the production of tb final state events is directly sensitive to contributions from extra W bosons or charged Higgs bosons as predicted in two Higgs doublet model (2HDM).

The event selection is presented in three steps. A first one makes use of a standard cut-based analysis, and will serve as a reference with the early data. In a second step, likelihood functions designed to improve the discrimination against specific backgrounds are presented together with the sets of discriminant variables that enter their definition. Finally, the selection criteria applied on those likelihoods are defined so that the total uncertainty affecting the cross section determination is minimized.

7.1 Sequential cut analysis

After applying the common preselection described in Section 5, a selection has been defined in order to account for the specific topology of s-channel events. Only two-jet events are considered, and a jet veto on any other jet above 15 GeV is applied. This strong requirement is used to reject $t\bar{t}$ events which represent the dominant background to our signal at this stage. Both jets are then required to be positively identified as b jets. This requirement reduces the W+jets and QCD multijet contamination, since those events feature much softer b jets or no b jets at all. The left plot in Fig. 18 shows the opening angle $\Delta R(b,b)$ between the two b-tagged jets in the event. In the W+jets production, this angle is expected to be small because of the reduced available phase space of the second b jet. On the contrary b jets in top pair production are expected to have a large opening angle and be almost back-to-back.

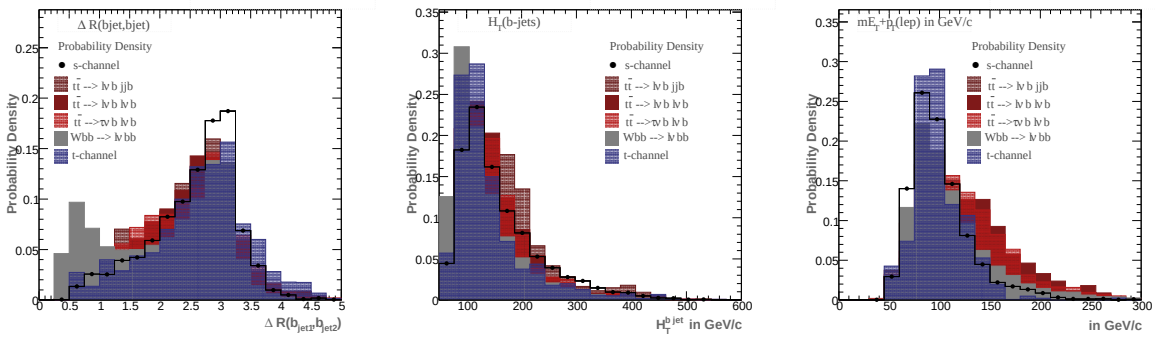

Figure 18: Probability density functions for the three variables used in the cut based analysis. From left to right: $\Delta R(b_1,b_2)$ the opening angle between the two b jets; H_T^{jet} scalar sum of jet transverse momenta; $p_T^{lep}+mE_T$ the sum of the lepton p_T and missing transverse energy. Cuts are indicated in the text.

The center plot in Fig. 18 displays the invariant mass formed from the two b jets in the events. The upper bound on this variable is aimed at reducing the contamination from top pair events, while the lower bound decreases the contribution from low energy W+jet events. The right plot in Fig. 18 shows the sum of the lepton transverse momentum and the missing transverse energy. Top pair events, specially in the *dilepton* channels, tend to have more missing energy due to the presence of extra neutrinos. The selection requires the opening angle between the two jets to be: $0.5 < \Delta R(b,b) < 4.0$, the scalar sum of

total jet transverse momenta $H_T(jet)$ to be $80 \leq H_T(jet) \leq 220$ GeV and finally the sum of the transverse missing energy and lepton transverse momentum to be ranging between $60 < \not{E}_T + p_T(lep) < 130$ GeV.

Selected event yields are reported in Table 10 for the three single top processes, and all $t\bar{t}$ and W+jets backgrounds. When adding all contributions, the signal overall efficiency is about 1.1% in the electron channel and 1.6% in the muon channel. This corresponds to a total of about 25 selected candidates for an integrated luminosity of 1 fb^{-1}. The S/B ratio is about 10%. The dominant background is composed by the $t\bar{t}$ events which account for about 60% of the total background yield. Among those, the $t\bar{t}$ in the lepton+jets mode, including τ decays, contribute about 40%. The remaining backgrounds originate from the $Wb\bar{b}$+jets production, which constitutes about 14% of the background yield, and almost equally from the single top t-channel (11%) and W+jets (9%) events. As expected, W+jets events are removed because of the requirement of b-tagged jets, with a final yield depending upon the mistag rate. Diboson contributions (WW and WZ) are found negligible.

Events in 1fb^{-1}	e channel	μ channel	$e+\mu$ *combined*
s-channel	10.3 ± 0.8	14.5 ± 1	24.8 ± 1.3
t-channel	17.0 ± 5.7	13.6 ± 5.1	30.6 ± 7.9
Wt-channel	6.5 ± 1.9	2.4 ± 1.2	8.9 ± 2.3
$t\bar{t} \to l + jets$	18.8 ± 4.3	20.5 ± 5.3	39.3 ± 5.3
$t\bar{t} \to ll$	29.0 ± 5.5	15.4 ± 5.0	44.4 ± 7.4
$t\bar{t} \to l\tau$	20.5 ± 5.6	40.9 ± 6.9	61.4 ± 8.9
$Wb\bar{b}$+jets	18.9 ± 2.0	19.7 ± 2.0	40.6 ± 2.5
W+jets	14.8 ± 1.4	11.0 ± 2.2	25.8 ± 2.3
Total Bkg	125.5 ± 10.3	123.5 ± 10.6	251.0 ± 14.2
S/B	8.2%	11.7%	9.8%
$S/\sqrt{B}$	0.92	1.3	1.6

Table 10: *Event yield for signal and background for the cut-based analysis in the 2-jet multiplicity bin for 1 fb^{-1}. Uncertainties come from Monte Carlo statistics only.*

7.2 Likelihood selection

The cut based analysis shows that a simple approach to select single top s-channel events is hampered by a high level of background. The use of a likelihood discriminator is aimed at improving the performance of the discrimination against backgrounds in order to purify the selected samples. This approach assumes that the distributions entering the definition of likelihood functions are well known and validated on data itself. This result can be achieved by cross-checking at every step the agreement between data and Monte Carlo generators on selected sub-samples where a high level of background is expected. In the following, only pre-selected events with exactly two jets, both of which are b tagged are considered.

7.2.1 Definition of the likelihood functions

The main background processes to our signal show very distinct features in final state and topology that lead us to define several likelihood functions each devoted to the discrimination of a specific process: three likelihood functions are devoted to $t\bar{t}$ events in the dilepton, the $l+\tau$ and the l+jets decay modes and two likelihood functions have been formed to discriminate against W+jets and t-channel events. Because of the limited Monte Carlo statistics, these likelihood discriminators have been defined by combining both muon and electron channels.

Variable	$\mathscr{L}_{t\bar{t}/l+jets}$	$\mathscr{L}_{t\bar{t}/dilepton}$	$\mathscr{L}_{t\bar{t}/l\tau}$	$\mathscr{L}_{W+jets}$	$\mathscr{L}_{t-channel}$
$H_T(b\ jets)$	X	–	X	X	X
$\Delta R(b,b)$	X	X	X	X	X
$M_{inv}(b,b)$	X	–	X	X	–
$\Delta\eta(l,b_1)$	X	X	X	X	X
$\Delta\eta(l,b_2)$	X	X	X	X	X
$\cos\phi(b_1,b_2)$	X	X	X	X	X
$M(W,b_1)$	X	X	X	–	X
$M(W,b_2)$	X	X	X	X	–
$p_T(b_1)$	X	–	–	X	X
$p_T(b_2)$	X	–	–	X	X
$mE_T + p_T(lep)$	X	X	X	X	–
$\Delta R(l,b_1)$	X	X	–	X	X
$\Delta R(l,b_2)$	X	X	X	X	X
$\cos\Phi(l,b_1)$	X	X	X	–	–
$\cos\Phi(l,b_2)$	–	–	X	X	–
$p_T(top1)$	X	–	–	X	X
$p_T(top2)$	X	–	–	X	X

Table 11: *List of variables entering the definition of the individual likelihood functions in the two-jet final state s-channel analysis*

The list of variables entering a likelihood function is derived from a procedure of optimization that selects only the variables that bring a signifi cant discrimination between signal and the considered background. The discriminating power of a given variable is computed using the selection effi ciencies for both signal and background in the plane $(\varepsilon_S, \varepsilon_B)$. The quantity corresponding to the difference of the area delimited by the median curve (equal selection effi ciencies $\varepsilon_S = \varepsilon_B$) and the area delimited by the $(\varepsilon_S, \varepsilon_B)$ curve can be seen as an estimator of the discriminating power of the variable. In this analysis, the variable is selected if the discriminating power is above 4%. The set of discriminant variables is constituted of 16 variables: the opening angles between the lepton and the jets $\Delta R(l,b_1)$, $\Delta R(l,b_2)$ and between the b jets themselves $\Delta R(b_1,b_2)$ as well as $\cos\Delta\Phi(l,b_1)$ and $\cos\Delta\Phi(l,b_2)$; the pseudo-rapidity of the b jets η_{b1} and η_{b2}; the invariant mass formed by the systems of the two b jets $M_{inv}(b_1,b_2)$ and by the reconstructed W leptonic boson and the b jets $M(W_{lep},b_1)$ and $M(W_{lep},b_2)$; the transverse momentum of the reconstructed top quark candidates $p_T(top_1)$ and $p_T(top_2)$; the sum of the missing transverse energy and lepton transverse momentum $\not{E}_T + p_T(l)$; the transverse mass of the leptonic W boson candidate $M_T(W_{lep})$; the scalar sum of the jet transverse momenta $H_T(jets)$; fi nally global event variables like sphericity, aplanarity and centrality, have been used.

7.2.2 Optimization of the likelihood selection

The likelihood function distributions corresponding to an integrated luminosity of 1 fb^{-1} are shown in Figure 19. We choose to apply simple thresholds on each of the 5 likelihood values. In the present

analysis, the thresholds on the likelihood values have been set so that the total uncertainty affecting the cross section measurement is minimized. We use the cross section expression given by:

$$\sigma_{s-channel} = \frac{N_{tot} - B}{a \times \mathscr{L}}$$

where N_{tot} is the sum of our signal and background events provided presently by Monte Carlo, B is the sum of all background contributions, a is the signal acceptance and $\mathscr{L}$ is the luminosity. The total uncertainty was calculated as described in Section 6.2.3. The main sources of systematics taken into account are the b-tagging, jet energy scale, luminosity and uncertainties on the background level, for which central values are provided in Section 7.3. Note that we consider the errors as fully correlated between signal and background for JES, b-tagging, and luminosity. The resulting thresholds on the likelihood functions are listed below:

$$\mathscr{L}_{t\bar{t}/lepton+jets} \geq 0.34 \ , \ \mathscr{L}_{t\bar{t}/dilepton} \geq 0.56 \ , \ \mathscr{L}_{t\bar{t}/\tau+lepton} \geq 0.80 \ , \ \mathscr{L}_{W+jets} \geq 0.32 \ , \ \mathscr{L}_{t-channel} \geq 0.46$$

Table 12 reports the number of events expected for all signal and backgrounds for an integrated luminosity of 1 fb^{-1}. The overall S/B ratio is improved significantly compared to the sequential cuts analysis with a purity increased from 9.8% to 18.7%. This is an expected outcome of the optimization procedure since the main source of uncertainty comes from the impact of b-tagging and JES uncertainties affecting the background.

Events in 1fb^{-1}	*e channel*	*μ channel*	*e + μ combined*
s-channel	6.3± 0.7	9.1±0.8	15.4± 1.0
t-channel	negl.	1.7 ±1.7	1.7 ± 1.7
Wt-channel	1.8±1.0	negl.	1.8 ± 1.0
$t\bar{t} \to l + jets$	7.6±2.6	7.7±3.5	15.3± 3.5
$t\bar{t} \to ll$	6.0±2.6	6.0±2.6	12.0± 3.8
$t\bar{t} \to l + \tau$	6.8±3.4	14.5±4.1	21.3±5.3
$Wb\bar{b}$+jets	10.0±3.2	7.0±2.6	17.0±4.1
W+jets	6.2±1.2	7.3±2.1	13.5±3.9
$WZ + WW$	negl.	negl.	negl.
Total Bkg	36.8 ± 5.8	45.9±6.6	82.7±8.6
S/B	17.3%	19.8%	18.7%
$S/\sqrt{B}$	1.0σ	1.3σ	1.7σ

Table 12: *Number of expected events for an integrated luminosity of 1 fb^{-1} expected from the likelihood analysis in the two jet final state events. The results are shown separately for the electron and muon channels. Statistical uncertainties correspond to the Monte Carlo statistics only.*

The dominant background comes from $t\bar{t}$ production, which contributes about 60% of the total event yield. Among those events, the main contribution originates from the $l + \tau$ decay modes, which corresponds to 45% of the $t\bar{t}$ yield, followed by the dilepton and the l+jets channels. The production of $Wb\bar{b}$+jets represents about 20%, while the W+jets events still contribute 16% of the total background yield. Finally, the contamination originating from the other single top channels is smaller than the signal expected event yield with a contribution of 4% from the sum of t- and Wt-channel channels.

A 5 σ (3 σ) discovery requires about 8.6 fb^{-1} (3 fb^{-1}). The results show a similar statistical sensitivity compared to the standard cut-based analysis, with an improved S/B ratio. As described in Section 4 the presence of pile-up affects the reconstruction of the objects selected in the event. The use of events with pile-up results in a decrease of about 9% for signal events, and 15% for $t\bar{t}$ events. We consider that a global factor of 85% must be applied to the event yield reported in Table 12.

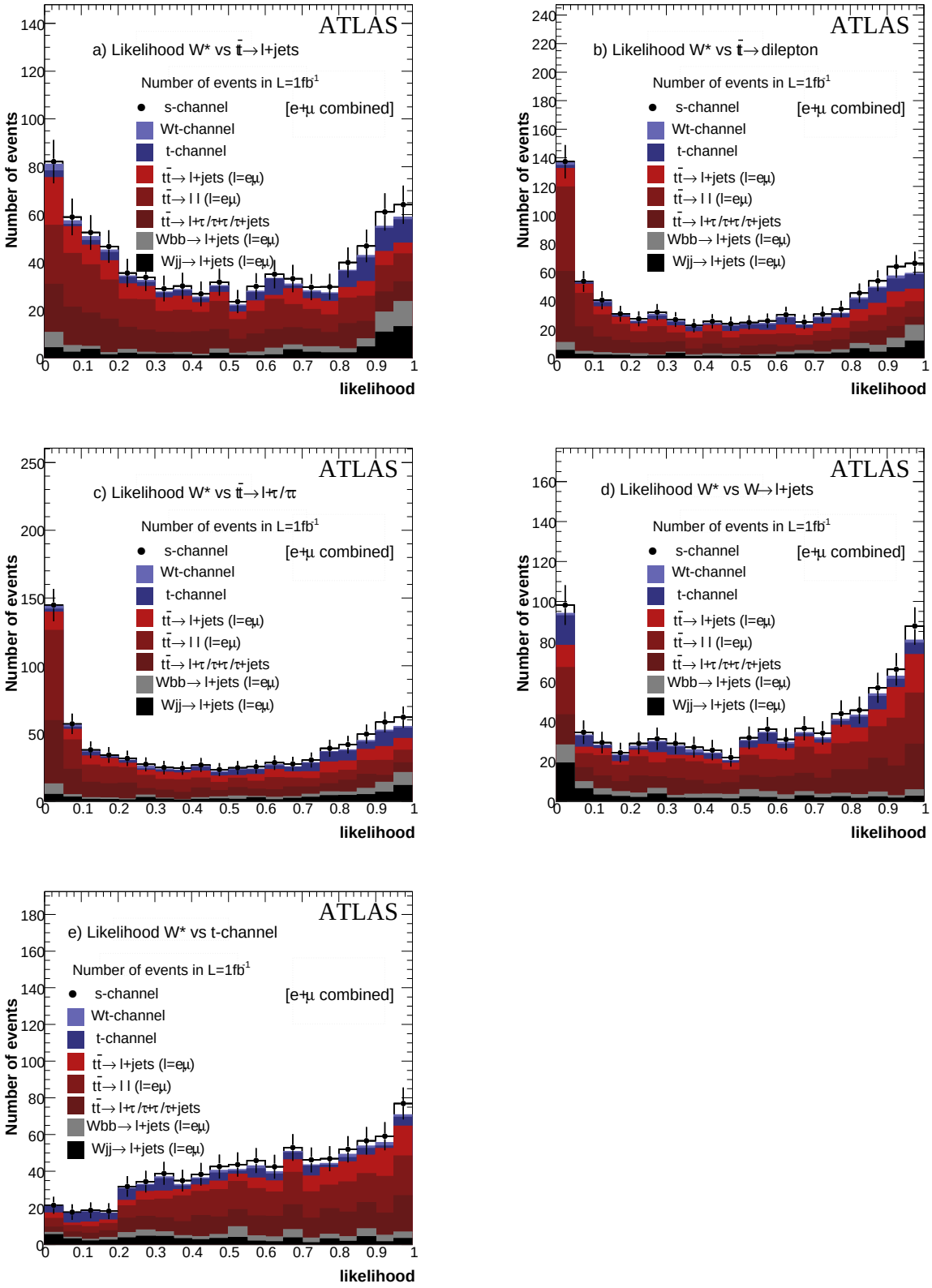

Figure 19: Distributions of the five likelihood functions for an integrated luminosity of 1fb^{-1}. a) Likelihood against $t\bar{t}$ in the l+jets channel; b) Likelihood against $t\bar{t}$ in the dilepton channel; c) Likelihood against $t\bar{t}$ in the $l+\tau$ channel; d) Likelihood against W+jets events; e) Likelihood against t-channel events

7.3 Systematic uncertainties

7.3.1 Experimental systematic uncertainties

The uncertainties on the *b*-tagging efficiency and the mistag rates have been estimated by varying the *b* weight cut value corresponding to a change of $\pm 5\%$ in the *b*-tag efficiency. Table 13 shows the impact of such effects on signal and background events. As the *b*-tag efficiency is varied by +5% and -5%, the signal selection efficiency is shifted by 7.1% and -7.7% respectively. For background events, the impact of such variations result in both cases in an increase of the background level which reaches +15% and +5% respectively because of the change affecting the mistag rates. Table 15 reports the impact on the total cross-section determination. The understanding of the *b*-tagging performance completely drives the analysis strategy.

Number event ($1 fb^{-1}$)	*b*-tag -5%	*b*-tag +5%	JES -5%	JES +5%
s-channel	14.2 (-7.7%)	16.5(+7.1%)	16.9 (+9.7%)	15.4 (negl.)
t and Wt-channel	6.9 (+97%)	3.5 (negl.)	5.1 (+45%)	5.1 (+45%)
$t\bar{t}$ combined	47.8 (-1.6%)	58.1 (+19.5%)	49.5 (+1.8%)	46.9 (-3.5%)
$Wb\bar{b}$+jets	15.5 (-8.8%)	16.4 (-3.5%)	17.0 (negl.)	17.0 (negl.)
W+jets	17.0 (+26%)	17.0 (+26%)	15.4 (+14%)	15.1 (+11.8%)
Total bkg	87.2 (+5.4%)	94.9 (+14.8%)	87.7 (+6%)	84.9 (+2.6%)

Table 13: *Effect of the main systematic effects, b-tag efficiency and mistag rate variation and of the jet energy scale variation on the number of expected events for an integrated luminosity of 1 fb^{-1} expected from the likelihood analysis in the two jet final state events. Number in parenthesis are the percentage errors.*

A variation of -5% and +5% of the jet energy scale has been propagated to the jet reconstruction and the selection efficiencies were re-assessed. Changes of 9.7% and 0% are found in the signal events respectively, while the total background changes by about 6.0% and 3% respectively. Again, in both cases the background is increased with any change of the JES. Indeed, as the jet scale factor is decreased, top pair events in the dilepton and *l*+jets modes tend to have a lower multiplicity, resulting in an increased contamination. As the scale factor goes up, the low multiplicity events are favored while top pair production is almost not affected. Table 13 shows the effects of the JES variation on the signal and background event yield while Table 15 reports the impact on the total cross-section determination.

An uncertainty of 1% in the lepton identification or in the trigger efficiency would impact the number of selected events. Such an uncertainty would reflect in an uncertainty of 6% on the total cross-section measurement.

7.3.2 Theoretical and Monte Carlo systematic uncertainties

In the present analysis, uncertainties on the background estimates come from the theoretical uncertainties associated with their cross section. Our background sample is being constituted by $t\bar{t}$ events at 60%, by $Wb\bar{b}$+jets at 20% and by W+jets at 16%, a 10% uncertainty on the $t\bar{t}$ cross-section prediction and 20% on the W+jets and $Wb\bar{b}$+jets events leads to a total of 10.3% on the summed background. The understanding of the background level is thus a crucial point for a precise cross-section determination.

The selection of a 2-jet final state is very sensitive to the presence of extra jets originating from gluon radiations. Any uncertainty in the ISR/FSR modeling is thus expected to have a significant impact on

the selection efficiencies, in particular for the s-channel and the $t\bar{t}$ events. Specific Monte Carlo samples have been generated with ISR/FSR settings leading to the largest cross section variations. Variations of 5% of the signal selection efficiencies are expected, and are due to the change in the jet multiplicity. The uncertainties however reach large values for the $t\bar{t}$ productions, with variations of 17.8% between the two extreme cases. We therefore halve this variation and quote an overall 9% uncertainty due to the gluon radiation. We note that the variations have been assessed with non-calibrated jets, although there is a high expected correlation between JES and ISR/FSR gluon modeling. The s-channel being produced via quark-quark mechanisms, some constraints coming from the use of W boson events should allow the tuning of the showering interfaces.

Another uncertainty is related to to the choice of the PDFs. Table 14 reports the variations in the selection efficiencies for the s-channel and the top pair production, which constitutes the dominant background to the analysis. The expected bias on the signal is 2% while this number is about 3% for $t\bar{t}$ events.

Channel / Final State	ε (%)	$\Delta\varepsilon^{+}(\%)$	$\Delta\varepsilon^{-}(\%)$	Generator+PDF
s-channel / $e^{\pm}\nu_e(\bar{\nu}_e)$	1.977	1.165%	1.702%	AcerMC+CTEQ6.1
s-channel / $\mu^{\pm}\nu_\mu(\bar{\nu}_\mu)$	2.259	1.200%	1.737%	AcerMC+CTEQ6.1
s-channel / $\tau^{\pm}\nu_\tau(\bar{\nu}_\tau)$	0.201	1.271%	1.749%	AcerMC+CTEQ6.1
$t\bar{t}$ / $l^{\pm}\nu_l(\bar{\nu}_l)+q\bar{q}$	0.086	2.472%	3.179%	MC@NLO+CTEQ6.1

Table 14: Single top different channel/final state selection efficiency uncertainties (absolute and relative scale) due to PDF uncertainties. For each channel, the uncertainty in the semi-leptonic $t\bar{t}$ background selection is also shown. The values are obtained using the re-weighting method.

Finally the effect of the b-fragmentation parameterization has also been investigated. The b quark fragmentation is performed according to the Peterson parametrization, with one free parameter ε_b. Varying the default value from $\varepsilon_b = -0.006$ by ± 0.0025 [53] and taking the difference as a systematic uncertainty leads to a change of 3.6% in the $t\bar{t}$ and signal selection efficiencies.

7.3.3 Systematic uncertainties and impact on cross-section

Table 15 lists all sources of uncertainties and reports their impact on the cross-section determination. Two cases are considered : one defined by the level of uncertainty in the b-tagging, JES, luminosity that will presumably characterize the early data taking period and a second one assuming a reasonable improvement on those effects with an integrated luminosity of 10 fb^{-1}.

Monte Carlo statistics is an important source of uncertainty, exclusively because of the lack of background sample, given the high rejection factors obtained in our selection. The uncertainty from the data statistics with a luminosity of 1fb^{-1} is the result of the Poisson law used to describe the expected signal and background event yields. A 5% uncertainty in the luminosity results in a 31% relative error in the cross-section determination because of the low S/B ratio. The estimate of background events is of crucial importance, and will be data driven, since the knowledge of the main backgrounds $t\bar{t}$ and W+jets is already theoretically limited to levels well above 10%. Among the main sources of systematic uncertainties, the b-tagging performance is the dominant one, since a double-btag requirement is used in our analysis. A precise knowledge of the JES will also impact our analysis, since the best discriminant variables depend upon the JES.

7.4 Summary

The determination of the s-channel cross section constitutes a challenging measurement, because of a large background from the $t\bar{t}$ production and from the W+jets events. With an expected ratio S/B of

18% the measurement will be hampered not only by a significant statistical uncertainty but also by the systematic effects affecting both signal and background. The measurement with an integrated luminosity of 1 fb^{-1} is both statistically and systematically limited, with about 60% of statistical errors and 80% of systematic uncertainties.

Given the present limitation on the background knowledge, early measurements will have to be devoted to the understanding of the backgrounds, in terms of shape and absolute normalization. In this area, the knowledge of the effects of the ISR/FSR gluon radiation will need devoted studies, in particular in $t\bar{t}$ events. The constraint from data itself will thus be very important, and a tuning *à la* CDF [54] will be crucial for the understanding of these radiations. From the detector side, a reliable cross-section measurement requires a good knowledge of the *b*-tagging tools performance, since double-tag events are considered. A good determination of the jet energy scale is also mandatory for the selection, at the level of better than 5%. PDF and *b*-fragmentation effects are expected to have a more significant impact only at higher luminosity.

In this context, the use of sophisticated statistical methods appears mandatory to discriminate the signal from the background and to reach an evidence of the signal. Their use however require an a priori good understanding of the background normalization and shapes. With an improved situation for the *b*-tagging, JES, with a background normalization determined from the data and a better ISR/FSR knowledge, the present analysis can lead to an evidence at 3 σ for about 30 fb^{-1}.

Source of uncertainty	Analysis for 1 fb^{-1} Variation	$\Delta\sigma/\sigma$	Analysis for 10 fb^{-1} Variation	$\Delta\sigma/\sigma$
Data Statistics		64%		20%
MC Statistics		29%		
Luminosity	5%	31%	3%	18%
b-tagging	5%	44%	3%	25%
JES	5%	25%	1%	5%
Lepton ID	1%	6%	1%	6%
Bkg x-section	10.3%	47%	3%	16%
ISR/FSR	9%	52%	3%	17%
PDF	2%	16%	2%	16%
b-fragmentation	3.6%	19%	3.6%	19%
Total Systematics		95%		48%

Table 15: *Summary of all uncertainties that affect the measured cross section. Data statistics is the poisson error one would expect from real data while MC Statistics is the uncertainty on the estimated quantities due to MC statistics.*

8 Measurement of the Wt-channel cross section

The Wt-channel is characterized by the associated production of a top quark and a W boson. At the LHC, this single top process is the second of importance after the t-channel production, with an expected cross section of 66 pb. The corresponding final state features two W bosons and a b jet, making this channel experimentally very close to top pair production, from which it differs by the absence of a second b jet in the final state. With a cross section 15 times larger than the Wt-channel processes, top pair events will thus constitute the dominant source of backgrounds and drive the definition of the selection criteria in higher jet multiplicity events. On the other hand, low jet multiplicity events will suffer from the W+jets contamination. In this report, we consider only the case where one of the two bosons decays into leptons while the other decays into jets. Two approaches have been used to estimate the sensitivity to the Wt-channel cross section measurement: a sequential cut-based analysis, which will provide reference numbers, and an analysis based on the use of Boosted Decision Trees.

8.1 Sequential cuts analysis

The common preselection defined for all three single top processes has been extended further to account for the specific topology of Wt-channel events. Selected events must have exactly one high p_T b jet above 50 GeV . A veto on any other b tagged jet above 35 GeV is then applied in order to reject $t\bar{t}$ events. This b-tag veto utilizes a looser b-tag weight cut which has been optimized according to the signal over $t\bar{t}$ background ratio. Fig. 20 displays this ratio S/B as function of the b tag weight applied to the veto jet. The value optimizing the S/B is found to be around -2, for which the S/B is 18% in both the 2- and 3-jet final states and 14% in 4-jets events. The corresponding efficiency is about 30% on signal events and 10% on $t\bar{t}$ events, as shown in Fig. 21.

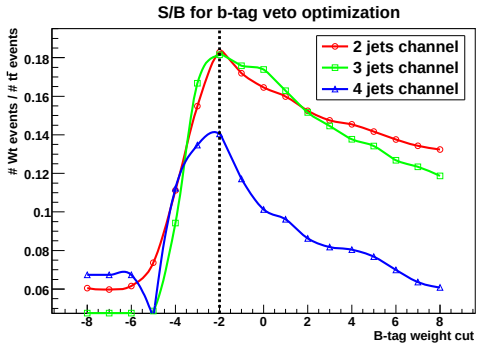

Figure 20: Signal over Background as function of the b tag weight cut selected for the secondary b tag veto.

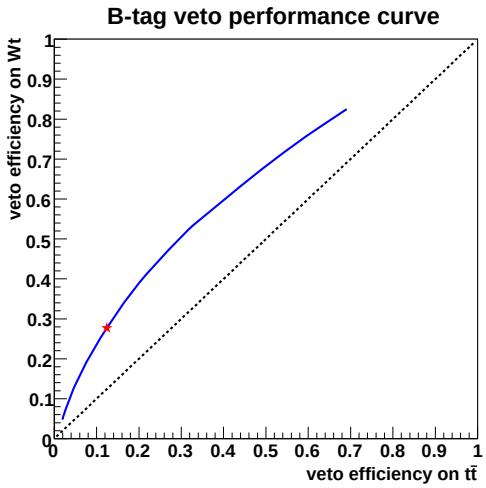

Figure 21: Veto efficiency for top pair events versus selection efficiency for Wt signal. The star indicates the efficiencies corresponding to the threshold used in the analysis

For events containing more than three high p_T jets, the selection requires that the invariant mass formed by the two leading untagged jets to be in a window: $50 \leq M(j_1, j_2) \leq 125$ GeV . The number of selected events is reported in Table 16 for signal and backgrounds.

In two jet events ('1b1j'), the signal yield is about 430 signal events for an integrated luminosity of 1 fb^{-1}, with a ratio S/B of 6.8%, combining both electron and muon channels. The W+jets production is the dominant background with more than 45% of the total background yield. The $t\bar{t}$ contamination in the l+jets channel constitutes about 20% of the background, while the other $t\bar{t}$ modes combined contribute 11%. In this low jet multiplicity bin, the single top t-channel contamination is significant and represents 19% of the total.

In three jet final state events ('1b2j'), 160 signal events are expected in 1 fb^{-1}, with a ratio S/B close to 15%. In this final state, the use of the hadronic W boson mass constraint helps improving the rejection of W+jets and the other single top events. The background is made up by $t\bar{t}$ events which represent 70% of the total background yield, and by about 20% of W+jets events. Among $t\bar{t}$events, the l+jets modeis dominant and constitutes about 85% of the total.

The four jet final state events ('1b3j') only brings a marginal improvement of the analysis. The number of expected Wt-channel single top events is small and expected to be 40 for 1 fb^{-1} and a ratio S/B of 10.6%. In this high jet multiplicity bin, the main background comes from the $t\bar{t}$ events in the l+jets mode, which constitute 64% of the background, the rest originating mostly from the single top t-channel and from W+jets events, each of the same order as the signal.

Nb events in 1fb^{-1}	2 jets (1b1j)	3 jets (1b2j)	4 jets (1b3j)
Wt-channel	435 ± 16	164 ± 10	40 ± 5
t-channel	1218 ± 47	94 ± 13	58 ± 11
s-channel	42 ± 2	5 ± 0.6	0.6 ± 0.2
$t\bar{t} \to l + jets$	1260 ± 38	664 ± 27	240 ± 16
$t\bar{t} \to dilepton$	291 ± 18	50 ± 7	17 ± 4
$t\bar{t} \to l + \tau$	428 ± 22	55 ± 8	17 ± 5
W+jets	2983 ± 71	207 ± 19	38 ± 6
$Wb\bar{b}$+jets	137 ± 33	13 ± 3	6 ± 2
TOTAL bkg	6359 ± 232	1088 ± 74	377 ± 42
S/B	6.8%	15.0%	10.6%
$S/\sqrt{B}$	5.4	5.0	2.1

Table 16: *Number of expected events for an integrated luminosity of 1 fb^{-1} as function of the jet multiplicity and for the electron and muon channel combined in the sequential cut-based analysis. Errors shown are statistical only.*

8.2 Boosted decision tree analysis

As in the s-channel analysis, several multivariate discriminators have been defined to optimize the discrimination against backgrounds that are characterized by very distinct features. Two Boosted Decision Tree (BDT) functions are defined to separate signal and $t\bar{t}$ events, one devoted to the discrimination from the dominant l+jets channel $\mathscr{D}_{t\bar{t}/l+jets}$, and the other against the dilepton lepton channels $\mathscr{D}_{t\bar{t}/dilepton}$ including τ's. A function $\mathscr{D}_{W+jets}$ has been formed to separate signal from the W+jets sample, defined as the summed contribution from light and heavy flavor jets. A last BDT discriminator is devoted to the separation of the signal and the single top t-channel events $\mathscr{D}_{t-channel}$. The analysis being based upon events with jet multiplicity between two and four, specific BDTs have been defined in each jet multiplicity bin for each background. The electron and muon channels are being treated in a combined way, thus leading to the definition of 12 BDT discriminators in total.

8.2.1 Definition of the discriminant variables

The set of discriminant variables that has been used is presented in Table 11. It includes 25 variables: the opening angles between the lepton and the jets $\Delta R(l,b)$, $\Delta R(l,j_1)$, $\Delta R(l,j_2)$ where j_1, j_2 and j_3 are the untagged p_T ordered jets, and between the jets themselves $\Delta R(b,j_1)$, $\Delta R(b,j_2)$, $\Delta R(j_1,j_2)$ as well as $\cos\Delta\Phi(j_1,j_2)$; the pseudo-rapidity of the untagged jets η_{j2} and η_{j3}; the invariant mass formed by the sum of all jets $M_{inv}(jets)$ and by the reconstructed W boson and top quark candidates $M_{inv}(W+t)$; the mass of the hadronic W boson candidate $M(W_{had})$ as well as the sum of the missing transverse energy and lepton transverse momentum $\not{E}_T+p_T(l)$; the transverse mass of the leptonic W boson candidate $M_T(W_{lep})$ and of the systems formed by the b jet and the reconstructed W bosons $M(b,W_{had})$ and $M(b,W_{lep})$;

Variable	$\mathscr{D}_{t\bar{t}/l+jets}$	$\mathscr{D}_{W+jets}$	$\mathscr{D}_{t\bar{t}/ll+l\tau}$	$\mathscr{D}_{t-channel}$
p_z^ν	X	X	X	–
$\Delta R(lep,b)$	X	X	X	–
$\Delta R(lep,j_1)$	–	X	X	X
$\Delta R(lep,j_2)$	–	–	–	X
$\Delta R(b,j1)$	X	X	X	X
$\Delta R(b,j2)$	X	–	X	X
$\Delta R(j1,j2)$	–	X	X	X
$\cos\Delta\phi(j_1,j_2)$	–	X	X	X
η_{j2}	–	X	–	X
η_{j3}	–	X	–	–
$M_{inv}(jets)$	X	X	X	X
$M_{inv}(W+t)$	X	X	X	X
$mE_T+p_T(lep)$	–	–	X	X
$M(W_{had})$	X	X	X	X
$M_T(W_{lep})$	–	–	X	X
$M(b,W_{had})$	–	–	X	X
$M(b,W_{lep})$	X	X	X	X
Sphericity	–	X	X	X
Aplanarity	–	X	X	X
Centrality	X	X	X	X
$H_T(jets)$	X	–	–	X
$H_T(total)$	–	–	X	X
$p_T(b)$	–	–	X	–
$p_T(j_1)$	X	–	–	–
$p_T(j_2)$	–	X	X	X

Table 17: *List of variables entering the definition of the individual Boosted Decision Trees in the three jet final state*

the scalar sum of the jet transverse momenta $H_T(jets)$ and of all objects in the events $H_T(tot)$ as well as

the transverse jet momenta $p_T(b)$, $p_T(j_1)$, $p_T(j_2)$; the longitudinal momentum of the neutrino solution computed with the top quark mass; finally the global event variables, sphericity, aplanarity and centrality, have been used.

The BDT output distributions associated to each of the four backgrounds are represented in Figure 22 for the 3 jet final state analysis for the electron+muon channels for 1 fb^{-1}.

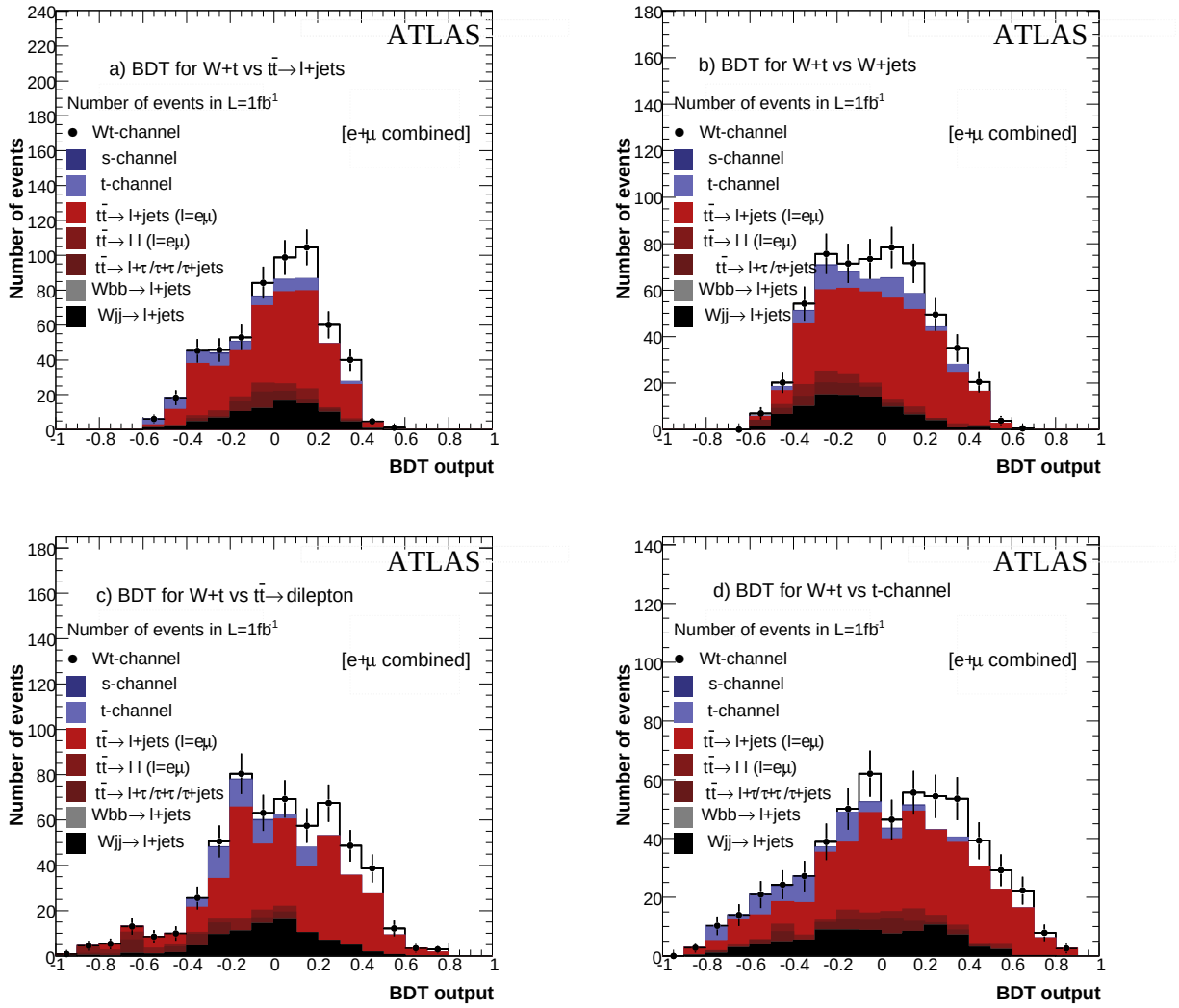

Figure 22: Distributions for the four BDT defined in the 3 jet ('1b2j') final state analysis. a) BDT against $t\bar{t}$ in the 'l+jets' channel; b) BDT against W+jets events; c) BDT against $t\bar{t}$ in the dilepton lepton (+tau) channel; d) BDT against single top t-channel events.

8.2.2 Results with the Boosted Decision Trees

Several selections can be designed, allowing for different levels of signal purity. In this analysis as in the s-channel, the cuts on the discriminant BDTs have been set so that the total uncertainty affecting the cross section measurement is minimized. The resulting thresholds for BDT outputs are:

$$\mathscr{D}_{ttlj} \geq 0.06,\ \mathscr{D}_{ttl\tau} \geq -0.36\ ,\ \mathscr{D}_{W\,jet} \geq 0.30\ ,\ \mathscr{D}_{t-chan} \geq 0.18$$

The number of events for signal and the different backgrounds is reported in Table 18 for an integrated luminosity of 1 fb^{-1}.

In two jet events ('1b1j'), the signal yield is about 60 signal events for an integrated luminosity of 1 fb^{-1} with a ratio S/B of 35%, combining electron and muon analyses. This result represents an improvement by a factor 6 in the S/B ratio compared to the cut-based analysis. This feature is important since one of the main sources of systematic uncertainty originates from the imperfect knowledge of the background levels. Regarding the composition of the background, the W+jets production constitutes the dominant background and contributes 58% of the background yield. $t\bar{t}$ production in the l+jets mode represents about 40% of the total. The only remaining single top events originates from the t-channel , which accounts for 6% of the total background yield. The statistical significance for this final state analysis alone is 4.5 σ.

In three jet final state events ('1b2j'), about 20 signal events are expected in 1 fb^{-1}, with a ratio S/B of 46%. Again, one notices a gain of more than a factor 3 compared to the cut-based analysis. The background events are made up almost exclusively of $t\bar{t}$ events in the lepton+jets events at 95%. The use of the jet-jet invariant mass reduces the W+jets background to a few percent. The selection in this final state alone provides a signal significance of 3.1 σ.

In the four jet final state events ('1b3j'), the number of expected Wt-channel single top events is 7 for 1 fb^{-1}. In this bin, the ratio S/B is about 42%, which corresponds to a gain of a factor 4 compared to the sequential cut analysis. In this jet multiplicity bin, the only competing processes is the $t\bar{t}$ events in the l+jets. The signal significance remains small, around 1.7σ with a corresponding statistical precision of 72%.

Nb events in 1fb^{-1}	2 jet (1b1j)	3 jet (1b2j)	4 jet (1b3j)
Wt-channel	58.0 $\pm$ 5.8	20.9 $\pm$ 3.5	6.6 $\pm$ 2.0
t-channel	10.2 $\pm$ 4.2	negl.	1.7 $\pm$ 1.7
s-channel	1.4 $\pm$ 0.3	negl.	negl.
$t\bar{t} \to all\,jet$	negl.	negl.	negl.
$t\bar{t} \to l + jet$	56.3 $\pm$ 8.2	41.8 $\pm$ 6.3	13.7 $\pm$ 3.4
$t\bar{t} \to dilepton$	1.7 $\pm$ 1.2	negl.	negl.
$t\bar{t} \to l + \tau$	negl.	negl.	negl.
W+jets	92.1 $\pm$ 8	3.2 $\pm$ 1.4	0.2 $\pm$ 0.1
$Wb\bar{b}$+jets	3.9 $\pm$ 3.9	negl.	negl.
TOTAL bkg	165.6 $\pm$ 9.2	45.1 $\pm$ 6.3	15.6 $\pm$3.4
S/B	35.0%	46%	36.2%
$S/\sqrt{B}$	4.5	3.1	1.7

Table 18: *Number of expected events for an integrated luminosity of 1 fb^{-1} as function of the jet multiplicity after the BDT analysis.*

The effect of pile-up has been investigated with signal and $t\bar{t}$ samples produced with a pile-up corresponding to a 10^{32} cm^{2}s^{-1} luminosity run. The results show a decrease of 18% for the signal event yield in the 2-jet final state, 47% in the 3-jet final state and 26% in the 4-jet bin. For backgrounds, similar variations are seen with 16% in the 2-jet bin, 39% in the 3-jet analysis and 20% in the 4-jet final state. As expected the increase of the number of light jets seen in the events directly impacts the tight selection of 2- and 3- jet final states. No systematic uncertainty is associated to this effect.

8.3 Systematic uncertainties

8.3.1 Experimental systematic uncertainties

The b-tagging uncertainties affect the Wt-channel selection because of the requirement of one b-tagged jet on one side, and the use of a veto for any second b jet on the other side. The variation by 5% of the b tagging efficiency and the corresponding mistag rate results in a 7% change of the signal selection efficiency in the 2 jet final state. The sensitivity is higher in the higher multiplicity bins, with effects of 10% seen in the 3-jet bin. Regarding backgrounds, the impact of this uncertainty increases with the bin multiplicity, with $t\bar{t}$ events being the dominant background. Variations of 3% and 5% are seen respectively in 3-jet and 4-jet final states. Table 19 reports the relative changes in signal and background events. Table 21 reports the impact on the total cross-section determination, all final states combined.

Process	N(1fb^{-1})	b-tag $\pm$ 5%	JES $\pm$ 5%
2-jet events			
signal	58.0	$\pm$ 7.0%	$\pm$0.5%
total bkg	165.6	$\pm$ 3.0%	$\pm$3.1%
3 jet events			
signal	20.9	$\pm$10.1%	$\pm$7.0%
total bkg	45.1	$\pm$3.2%	$\pm$3.0%
4 jet events			
signal	6.6	$\pm$3.1%	$\pm$7.9%
total bkg	15.6	$\pm$5.1%	$\pm$4.0%

Table 19: *Effect of the b-tag efficiency and mistag rate variation and of the JES variation on the number of expected events for an integrated luminosity of 1 fb^{-1} expected from the BDT analysis.*

The precise knowledge of the jet energy scale is important for the Wt-channel analysis because of the requirements made on the mass reconstruction and p_T thresholds used to select jets. A 5% variation of the jet energy scale has been propagated to the jet reconstruction and the selection efficiencies are re-assessed. Table 19 shows the impact of the JES variation on signal and background event yields. In two jet events, the effects of the JES variation is about 1% on the signal events and 3% on the sum of all backgrounds. In three jet events a variation of 7% of the signal event yield is observed, with a change of 3% in the backgrounds. In four jet events, strong variations of 8% and 4% are seen in signal and background respectively. Table 21 reports the impact on the total cross-section determination.

An uncertainty of 1% in the lepton identification or in the trigger efficiency would impact the number of selected events. Such an uncertainty would reflect in an uncertainty of 2.6% on the total cross-section measurement, which is negligible with respect to the others.

8.3.2 Theoretical and Monte Carlo uncertainties

Uncertainties on the background estimates come from the theoretical uncertainties associated to the cross sections. An uncertainty of 10% is quoted for the $t\bar{t}$ events while 20% is associated to the W+jets and $Wb\bar{b}$+jets events. This translates into a total 12.5% in the 2 jet final state and 10% in the higher jet multiplicity bins where $t\bar{t}$ events completely dominate the background.

The selection of a low jet multiplicity final state is very sensitive to the presence of extra jets originating from gluon radiations. Any uncertainty in the ISR/FSR modelling is thus expected to have a

significant impact on the selection efficiencies, in particular for the Wt-channel and top pair events. We quote an overall 9% uncertainty due to the gluon radiation in the $t\bar{t}$ events modelling.

The uncertainties in the PDF may affect the topologies as well as the momentum distributions of the final state objects, hence impacting the determination of the selection efficiency for both signal and backgrounds. The procedure to estimate the impact of the choice of the PDF to the selection efficiency is detailed in Section 4.4.3. Table 20 reports the variations in the selection efficiencies for the $s-channel$ events and the main top pair events, which constitutes the dominant background to the analysis. A 2% uncertainty results into a 3.8% contribution to the total systematic errors. Complete studies have been

Channel / Final State	ε (%)	(abs)$\Delta\varepsilon^+$	(abs)$\Delta\varepsilon^-$	$\Delta\varepsilon^+$ (%)	$\Delta\varepsilon^-$(%)
Wt-channel *channel* (2j) / $e^{\pm}\nu_e(\bar{\nu}_e)+q\bar{q}$	5.049	0.105	0.119	2.094	2.365
Wt-channel *channel* (2j) / $\mu^{\pm}\nu_{\mu}(\bar{\nu}_{\mu})+q\bar{q}$	5.340	0.118	0.132	2.217	2.480
Wt-channel *channel* (2j) / $\tau^{\pm}\nu_{\tau}(\bar{\nu}_{\tau})+q\bar{q}$	0.851	0.015	0.015	1.797	1.839
$t\bar{t}$ (2j) / $l^{\pm}\nu_l(\bar{\nu}_l)+q\bar{q}$	1.938	0.019	0.026	0.997	1.362
Wt-channel *channel* (3j) / $e^{\pm}\nu_e(\bar{\nu}_e)+q\bar{q}$	4.527	0.062	0.066	1.387	1.474
Wt-channel *channel* (3j) / $\mu^{\pm}\nu_{\mu}(\bar{\nu}_{\mu})+q\bar{q}$	4.930	0.059	0.065	1.215	1.323
Wt-channel *channel* (3j) / $\tau^{\pm}\nu_{\tau}(\bar{\nu}_{\tau})+q\bar{q}$	0.782	0.006	0.007	0.889	0.956
$t\bar{t}$ (3j) / $l^{\pm}\nu_l(\bar{\nu}_l)+q\bar{q}$	2.703	0.038	0.048	1.407	1.787
Wt-channel *channel* (4j) / $e^{\pm}\nu_e(\bar{\nu}_e)+q\bar{q}$	1.202	0.011	0.011	0.953	0.949
Wt-channel *channel* (4j) / $\mu^{\pm}\nu_{\mu}(\bar{\nu}_{\mu})+q\bar{q}$	1.343	0.011	0.012	0.844	0.914
Wt-channel *channel* (4j) / $\tau^{\pm}\nu_{\tau}(\bar{\nu}_{\tau})+q\bar{q}$	0.212	0.002	0.002	1.156	1.224
$t\bar{t}$ (4j) / $l^{\pm}\nu_l(\bar{\nu}_l)+q\bar{q}$	1.142	0.002	0.002	0.235	0.260

Table 20: $W+t$ channel selection efficiency uncertainties (absolute and relative scale) due to PDF uncertainties. For each channel, the uncertainty in the semi-leptonic $t\bar{t}$ background selection is also shown. The values are obtained using the re-weighting method with a CTEQ6.1 PDF error set

performed in each final state and an overall 2% uncertainty is quoted for both signal and $t\bar{t}$ events.

Finally the effect of the *b*-fragmentation parameterization has also been investigated following a similar procedure of that defined in Section 7.3.2. The relative uncertainties of the different channel and final state selection efficiencies due to the *b*-fragmentation uncertainty is found to be 3.6%.

8.3.3 Systematic uncertainties and impact on cross-section

Table 15 lists all sources of uncertainties and reports their impact on the cross-section determination. Two cases are considered : one defined by the level of uncertainty in the *b*-tagging, JES, luminosity that will presumably characterize the early data taking period and a second one assuming a reasonable improvement on those effects with an integrated luminosity of 10 fb^{-1}. As for the s-channel analysis, the estimate of background events is of crucial importance, and will be data driven, since the knowledge of the main backgrounds $t\bar{t}$ and W+jets is already theoretically limited to levels well above 10%. Among the main sources of systematic uncertainties, the b-tagging performance is the dominant one, since a single-btag coupled to a btag veto requirements are used in the analysis. A precise knowledge of the JES will also impact our analysis, since the best discriminant variables depend upon the JES.

Table 21 lists all sources of uncertainties and reports their impact on the cross-section determination. Two cases are considered : one defined by the level of uncertainty in the *b*-tagging, JES, luminosity that will presumably characterize the early data taking period; one assuming reasonable improvements on those effects with an integrated luminosity of 10 fb^{-1}.

Source of uncertainty	Analysis for 1 fb^{-1} Variation	$\Delta\sigma/\sigma$	Analysis for 10 fb^{-1} Variation	$\Delta\sigma/\sigma$
Data Statistics		20.6%		6.6%
MC Statistics		15.6%		
Luminosity	5%	20%	3%	7.9%
b-tagging	5%	16%	3%	6.6%
JES	5%	11%	1%	1.5%
Lepton ID	1%	2.6%	1%	2.6%
Bkg x-section	12.5/10%(*)	23.4%	3%	9.6%
ISR/FSR	9%	24.0%	3%	7.8%
PDF	2%	5.2%	2%	5.2%
b-fragmentation	3.6%	9.4%	3.6%	9.4%
Total Systematics		48%		19.4%

Table 21: *Summary of all uncertainties that affect the measured cross section. Data statistics is the poisson error one would expect from real data while MC Statistics is the uncertainty on the estimated quantities due to MC statistics.(*) background to 2j (12.5%) and 3j and 4j final states (10%)*

8.4 Summary

The determination of the Wt-channel cross section constitutes a challenging measurement with the early data, due to the presence of important $t\bar{t}$ and W+jets backgrounds. This measurement makes use of the events with a jet multiplicity between two and four jets. With a S/B ratio of about 30-40%, the analysis requires a good knowledge of the W+jets production in the lower multiplicity bins, and of the $t\bar{t}$ process in higher bins. The estimates of the shapes and normalization of those processes will have to rely upon the use of data. Strategies exist for QCD and W+jets events, but the discrimination against $t\bar{t}$ events remains as a challenge.

As the t-channel single top analysis, the cross section determination will be very early dominated by the systematic uncertainties. The dominant effect is constituted by the background uncertainties, followed by the modeling of the gluon radiation. From the detector side, the dominant source of uncertainty is the *b*-tagging because of the imperfect knowledge of the *b*-tag and *b*-tag veto effi ciencies as well as of the mistag rates. Another source is the determination of the jet energy scale, which affects the reconstruction of the W boson mass and all the jet energies used in the analysis. Note that the determination of the luminosity better than 5% is required in order to ensure a good measurement, or the use of ratio of different Wt-channel fi nal states [55] can be used as well with higher luminosity. A 3 σ evidence can be reached with a few fb^{-1} of data taking and a precision of 20% on the cross-section measurement is achievable with about 10 fb^{-1} provided that improvements are made in both the experimental aspects of the detection (backgrounds from data, *b*-tagging, JES and luminosity) and from the theoretical side.

9 Single top evidence with the early data

The early data are characterized simply by low luminosity levels, below 1 fb^{-1} , and the larger impacts of certain systematics, particularly jet energy scale and b-tagging systematics. The purpose of this analysis is to detect single top events, and thus an emphasis is placed on reaching a discovery-level significance at very low luminosities. It should also be noted that this analysis is not divided into separate channels, but rather looks at the combined single top signal.

9.1 Event selection

The typical preselection cuts discussed in previous sections were applied here, although because this is a low luminosity study, the second jet p_T cut was adjusted to 25 GeV the lepton p_T cuts were adjusted to 20 GeV for electrons and 25 GeV for muons, and the early data b-tagger, TRFIP2D, was used. Additionally, the trigger cuts could not be applied to the W+jets samples (not including $Wbb + jets$), since these were FastSim files, so these events were weighted based on the trigger turn-on curves instead. After applying these cuts, the events were separated into groups according to the number of b-tagged jets, specifically looking at 1 or 2 b-tagged jet events, effectively introducing a maximum tagged jet cut. The event yields, weighted to 100 pb^{-1} can be found in table 22 for samples containing 1 or 2 b-tagged jets, and muons or electrons.

processes	muon (1 b-jet)	muon (2 b-jet)	electron (1 b-jets)	electron (2 b-jets)
s-channel	13.9	8.4	9.9	6.4
t-channel	336.2	107.2	247.8	93.6
W+t channel	99.8	28.2	76.6	23.8
$t\bar{t} \to l + jets$	899.4	547.4	729.5	444.7
$t\bar{t} \to l + l$	411.0	270.3	316.8	205.7
$W + \ jets$	1422.8	113.9	878.7	79.1
$Wbb + 0 \ jets$	45.9	25.7	29.2	16.8
WW	23.1	3.3	17.9	1.9
WZ	7.3	2.8	5.4	2.2

Table 22: *Yields of reconstructed signal and background events at* 100 pb^{-1} *for muon and electron analysis, separated by number of b-tagged jets. Muon and electron both refer to isolated muons and electrons.*

9.2 Significance and luminosity

The significance values for several different low luminosity levels were examined without the addition of systematics and, at 100 pb^{-1} anticipated significance levels were estimated at 11.3σ for the 1 tagged jet sample and 6.5σ for the 2 tagged jet sample, even without cuts beyond the preselection cuts. A much more realistic estimate including systematics drops the anticipated significance levels at 100 pb^{-1} to 0.8σ for the 1 b-tag sample and 1.0σ for the 2 b-tag sample. Fig. 23 shows the significance value for each of the samples, including JES and B-tagging systematics. Here, the electron and muon samples are combined together, so that there are only two samples differentiated by number of tagged jets.

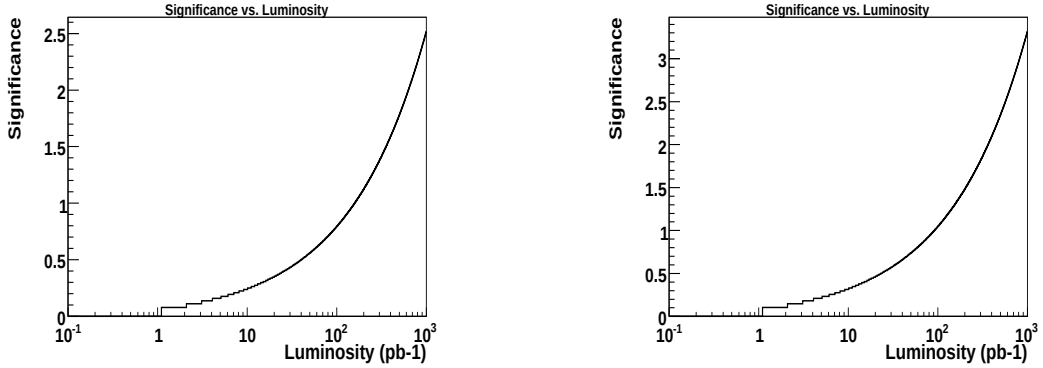

(a) (b)

Figure 23: $\frac{\text{signal}}{\sqrt{\text{background}}}$ *(significance) versus luminosity, for events containing (a) 1 b-tagged jet and (b) 2 b-tagged jets with a log scale, where signal is Wt, s-, and t channels combined and background is $t\bar{t}$ W+jets, Wbb+jets, WW, and WZ combined. These plots include both JES and b-tagging systematics*

9.3 Systematics estimation

In the previous section, it was apparent that it is possible to reach a discovery-level significance at low luminosities. However, these numbers represent an optimal running and understanding of the detector, since these numbers do not include systematics errors. Thus, it is prudent to examine sources of systematic errors and see what cuts can be made to reduce this error and bring us closer to these optimal numbers. The JES and b-tagging systematics were emphasized, because of their expected impact on early data.

To examine the JES systematic, the JES error was taken as 10 percent. The jet energies in the events were then scaled up and down by this percentage and the overall change in events from an unscaled sample was noted. The b-tagging efficiency was also altered up and down to determine the average effect of this systematic. These systematics were then squared and added to the number of background events in the $\frac{\text{signal}}{\sqrt{\text{background}}}$ calculation. In this way, the effect of this error on significance at a particular luminosity could be estimated. The effects of the JES and b-tagging systematics on the anticipated significance level at 100 pb^{-1} can be seen in table 23. This table also includes a brief look at numbers without b-tagging cuts, referred to as the no b-tag sample.

systematics	1 b-jet	2 b-jets	no b-jet
Statistical Error Only	11.3	6.5	9.3
JES	0.9	2.2	0.3
B-tagging	1.8	1.2	N/A
JES and B-tagging	0.8	1.0	N/A

Table 23: *Significance for the one and two tagged jet sample (at 100 pb), as well as a sample without b-tagging cuts, for different systematics. All samples include only the preselection cuts.*

9.4 Additional variable selection

Extra requirements were then examined to help reduce the systematic effects and increase the anticipated signifi cance levels. All the considered variables were scanned one at a time over the possible ranges of cut values to determine what cut value would result in the highest signifi cance value for a particular variable at a given luminosity. The best cut and corresponding signifi cance value for each variable were examined to determine an optimal fi rst cut (after preselection) to allow a higher potential signifi cance value at a given luminosity. This initial study was done only looking at cuts on individual variables, which include:

- H_T(jet1, jet2), H_T(all jets), H_T(lep, MET), H_T(jet1, jet2, lep, MET), H_T(all jets, lep, MET)
- Δp_T(jet1, jet2), Δp_T(btaggedjet1, untaggedjet1)
- ΔR(btaggedjet1, lep), ΔR(untaggedjet1, lep), ΔR(jet1, lep)
- ΔR(btaggedjet1, btaggedjet2), ΔR(jet1, jet2)
- H(all jets), H(jet1, jet2), *Missing* E_t (also written MET)
- p_T(jet1), p_T(btaggedjet1), p_T(untaggedjet1), p_T(untaggedjet2), p_T(lep), p_T(jet1) + p_T(jet2)
- η(btaggedjet1), η(untaggedjet1), Maximum jet eta in event, Minimum jet eta in event
- Number of jets, Number of untagged jets
- Transverse mass of W (W M_t), Mass of the b-tagged top, Mass of (jet1 + jet2)
- Centrality(all jets, lep),Centrality(jet1, jet2)

Additionally, plots normalized to 100 pb^{-1} are shown for a selection of variables including H_t and eta of the leading untagged jet in Fig. 24, and the top mass and leading lepton p_T in Fig. 25. The plots are shown for the 1 b-tag sample and do not include systematic effects.

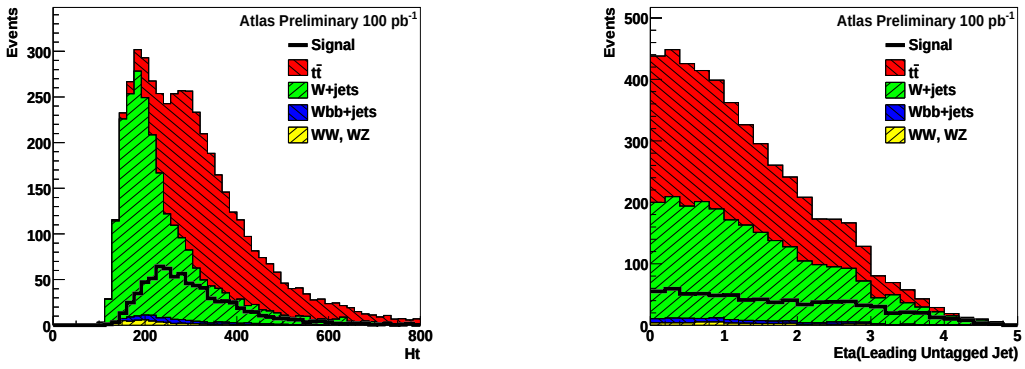

(a) (b)

Figure 24: H_t *(a) and eta of the leading untagged jet (b) for the 1 tagged jet sample at* 100 pb^{-1}

In the case of the number of jets variable, a jet number cut of 2 is not indicated for our combined signal sample, unlike the individual channel analyses done at higher luminosities. For example, looking at the 1 b-tag sample, Fig. 26 shows a peak in s-channel signal in the 2-jet bin with a relatively small background, whereas the signal is much lower in the 3 and 4-jet bins compared to background, so an

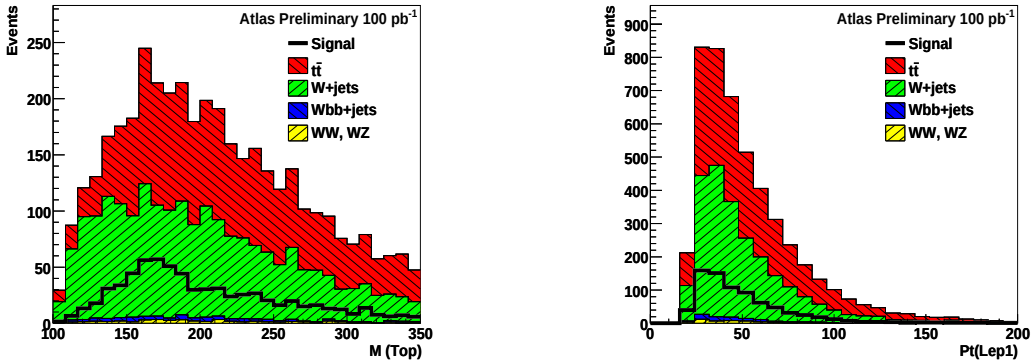

(a) (b)

Figure 25: *Top mass (a) and leading lepton p_T (b) for the 1 tagged jet smaple at* 100 pb^{-1}

analysis in this channel would require number of jets equal to two. However, the combined signals and the square root of the combined backgrounds do not vary much relative to each other. Thus, the combined signal and background study sees no useful cut to increase signifi cance here, in terms of improving statistical systematics, even though it may be very useful in a single channel analysis. If other systematics are also considered, then a jet number cut of 4 might be useful to reduce some of the effects of systematics, particularly JES systematics for the 1 b-tag sample.

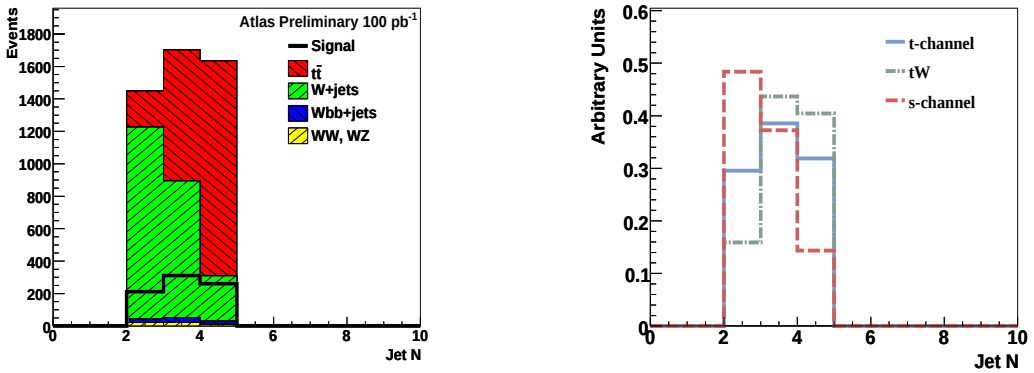

(a) (b)

Figure 26: *Number of jets in the 1 tagged jet sample normalized (a) to* 100 pb^{-1} *and (b) to unit area*

In the one and two b-tagged samples, including both JES and b-tagging systematics, certain cuts seemed useful, as can be seen in table 24. This analysis supported a cut requiring jet Number = 4 for the 1 b-tagged sample, which increased the potential signifi cance level to 1.4σ at 100 pb^{-1}. Also, a cut on the 2 b-tagged sample at leading untagged jet $|\eta| > 3.35$ raised the expected signifi cance level to 2.4σ at 100 pb^{-1}. Of course, we may not understand the detector well enough in early data to make a cut to keep such forward jets. In this case, the next best cut (of which there are several) has an anticipated signifi cance of about 1.1σ at 100 pb^{-1}. For early data, then, the 2 b-tagged sample, may require more complicated cuts.

samples	1 b-jet	2 b-jets
Preselection cuts	0.8	1.0
Preselection and best cut	1.4	2.4

Table 24: *Significance for the one tagged jet sample and the two tagged jet sample (at* 100 pb^{-1}*), with and without additional cuts, including both JES and b-tagging systematics. Best cut refers to* $\text{N(jet)} = 4$ *for the 1 b-tag sample and leading untagged jet* $|\eta| > 3.35$ *for the 2 b-tag sample. This eta cut may well be too forward for early data in the 2 b-tagged jet sample, in which case the next best cut would be associated with approximately* 1.1σ *significance*

9.5 Results

Thus, at 100 pb^{-1} without the inclusion of systematics, the estimated significance levels are above discovery level. These are the optimum levels however, and including the jet energy scale and b-tagging systematics at 100 pb^{-1} results in much lower anticipated significances. For the no b-tagging cut sample, the JES systematic resulted in a drop to an expected significance of 0.3σ. For the other two samples, including JES and B-tagging systematics, we anticipate significance levels of 0.8σ for a sample containing events with 1 b-tagged jets and 1.0σ for a sample containing events with 2 b-tagged jets. Initial work indicates that there may be cuts that can reduce the effect of these systematics. However, the large impact of these JES and B-tagging systematics shows that understanding them and finding additional cuts to lessen their impact will certainly play a large role in the analysis of early data.

10 Conclusion

At the LHC the production of single top events accounts for about a third of the $t\bar{t}$ production, which leads to about 2.5 million events per year during a low luminosity run at $10^{33}\text{cm}^2\text{s}^{-1}$. Similarly to the situation at the Tevatron, the selection of single top events will suffer from the presence of both W+jets and $t\bar{t}$ backgrounds, which are produced at much higher rates. Thus, careful approaches devoted to the understanding of these backgrounds in terms of shape and normalization performed directly from data will have to be defined. Besides, except for the s-channel, single top analyses will be very early dominated by the systematic uncertainties, and will require a good control of b-tagging tools and a reliable determination of the jet energy scale.

In a context of low signal over background ratio, the use of sophisticated tools like genetic algorithms, likelihoods and Boosted Decision Trees appears very useful if one wants to reach evidence of the signal with the early data or to determine precisely their cross-section. These techniques, which are now of current use at the Tevatron, will require the use of reliable event samples for modeling signal and backgrounds, that will presumably be produced from the data. The analyses should also be optimized with respect to the total level of systematic uncertainty, that will be the main limiting factor for 30 fb^{-1} measurements.

Finally, a precise determination of single top cross-sections can be achieved for a few fb^{-1} in the t-channel and the Wt-channel , while for the s-channel, a higher statistics will be required. Their interpretation in terms of new physics should thus come at a later stage, once the systematic effects are under control.

References

[1] Tait, T. M. P. and Yuan, C. -P., Phys. Rev. **D** (2001) 014018.

[2] D0 Collaboration, Phys. Rev. Lett. **98** (2007) 181802.

[3] CDF Collaboration, CDF/PUB/TOP/PUBLIC/8968 (2008).

[4] Abazov, V. M. (D0 Collaboration), Phys.Lett. B **641** (2006) 423–431.

[5] Abazov, V. M. (D0 Collaboration), Phys. Rev. Lett. **99** (2007) 191802.

[6] Sjostrand, T. and Mrenna, S. and Skands, P., JHEP **0605** (2006) 026.

[7] Corcella, G. and others, JHEP **0101** (2001) 010–103.

[8] Sullivan, Z., Phys. Rev. **D70** (2004) 114012.

[9] Campbell, J. and Ellis R. K. and Tramontano, F, Phys. Rev. **D70** (2004) 094012.

[10] Campbell, J. and Tramontano, F., Nucl. Phys. **B726** (2005) 109–130.

[11] Grebenyuk, O., Hadronic Single Top, Talk in ATLAS Top meeting.

[12] Kersevan, B. P. and Elzbieta, R. W., hep-ph/0405247 (2004).

[13] Slabospitsky, S. and Sonnenschein, L., Comput. Phys. Commun. **148** (2002) 87–102.

[14] Kersevan, B. P. and Hinchliffe, I., JHEP **069** (2006) 033.

[15] Frixione, S. and Weber, B. and Nason, P., hep-ph/0204244 and hep-ph/0305252 (2002).

[16] R. Bonciani et al., Nucl., Phys. **B529** (1998) 424–450.

[17] Hubaut, F. and Pralavorio, P., Eur.Phys. **C44S2** (2005) 13–33.

[18] Campbell, J. and Ellis, R. K., MCFM v5.0, 2006.

[19] Campbell, J. and Ellis, R. K. and Rainwater, D., Phys.Rev. **D68** (2003) 094021.

[20] Cooper, B. and Messina, A. and Waters, D., CDF note (2006).

[21] Dobbs, M. A., Phys. Rev. D64 **D64** (2001) 034016.

[22] Verkerke, W and Van Vulpen, I, Commissioning ATLAS using top-quark pair production, Internal Report ATL-COM-PHYS-2007-023, CERN, Geneva, Apr 2007.

[23] Abazov, V. M. and others, Phys. Lett. **B622** (2005) 265–276.

[24] Abazov, V. M. and others, Phys.Rev. D **75** (2007) 092007.

[25] ATLAS Collaboration, ATLAS Internal Notes **XXX** (2006).

[26] Cavalli, D. and others, ATL-COM-PHYS-2007-012 (2007).

[27] Shibata, A, ATL-COM-PHYS-2007-061 (2007).

[28] Shibata, A. and Clement, B., ATL-PHYS-PUB-2007-011 (2007).

[29] A. Lucotte, A. LLeres, F. Chevallier, ATLAS-PHYS-2007-005 (2007) 45 p..

[30] ATLAS Collaboration, CERN/LHCC/99-15 **2** (1999).

[31] ATLAS Collaboration, ATL-PHYS-PUB-XXX (2008).

[32] ATLAS Collaboration, ATL-SLIDE-2007-033 (2006).

[33] ATLAS Collaboration, ATL-SLIDE-2007-033 (2007).

[34] V.M. Budnev, Phys. Lett. **B39** (1972) 526–530.

[35] Dittmar, M. and Pauss, F. and Zurcher, D., ETHZ-IPP (1997) PR–97–01.

[36] Campbell, J.M, Huston, J.W., Stirling, W.J., Rept.Prog.Phys **70** (2007) 89.

[37] Cheng, T.L., in IOP HEPP Conference, University of Warwick, , 2006).

[38] J. Pumplin et al., Phys. Rev., D **65** (2001) 014013.

[39] A.D. Martin et al., Eur. Phys. J. **C28** (2002) 455–473.

[40] Stefan Gieseke, JHEP **0501** (2005) 058.

[41] Gwilliam, C B et al., ATLAS Internal Notes **ATL-COM-PHYS, 062** (2007).

[42] Peterson, C. and Schlatter, D. and Schmitt, I. and Zerwas, P. M., Phys. Rev. D **27** (1983) 105–111.

[43] B. Andersson et al., Z. Phys. **C20** (1988).

[44] M.G. Bowler, Z. Phys. **C11** (1981).

[45] ATLAS Collaboration, ATL-COM-PHYS-2008-XXX (2008).

[46] Clement, B. et al., ATL-COM-PHYS-2008-XXX (2008).

[47] Doxiadis, A., Kayl, M., ATL-COM-PHYS-2008-004 (2008).

[48] ATLAS Collaboration, ATL-COM-PHYS-2008-XXX (2008).

[49] D0 Collaboration, Phys.Rev. **D75** (2007) 092007.

[50] ATLAS Collaboration, CERN/LHC **99-14** (1999).

[51] BABAR Collaboration (P.F. Harrison and H. Quinn (editors) et al.), SLAC-R (1998).

[52] Kane, G.L. and Ladinsky, G.A. and Yuan, C. -P., Phys. Rev **D** (1992) 124–141.

[53] D. Abbaneo et al., ALEPH Collaboration, Phys. Rep. **294** (1998) 1.

[54] CDF Collaboration, Phys. Rev. D73 (2006) 032003, Sec. VII B.

[55] C.E. Gerber et al., FERMILAB-CONF **07-052** (2007) 125–138.